12

Extreme Variability of Relativistic Electrons in Earth's Outer Radiation Belt: An Overview and Recent Revelations

D. L. Turner and V. Angelopoulos

■ Abstract

This paper provides a brief history and general overview of observations of the extreme variability of Earth's outer radiation belt electrons. We compare and contrast observations and theory of the driving mechanisms responsible for drastic and rapid enhancements and depletions of relativistic electron intensity from the pre-CRRES (i.e., before 1990) and modern eras. The current understanding on dominant source, loss, and transport mechanisms responsible for extreme variations is presented. Particular emphasis is put on events such as rapid outer belt enhancements, sudden injections from interplanetary shock impacts, energetic electron injections from the plasma sheet, flux dropouts, and complex outer belt features like bifurcated drift orbits and double outer belts. Example cases of each type of event are provided from multipoint observations during the THEMIS and Van Allen Probes eras. We finish with a brief discussion on a few of the many outstanding questions and potentially interesting topics of future research.

Waves, Particles, and Storms in Geospace. First Edition. Georgios Balasis, Ioannis A. Daglis, Ian R. Mann.

12.1 Introduction

Earth's radiation belts were the first major scientific discovery of the space age. Based on observations from several of the world's first human-built satellites, Van Allen and Frank [1959] and Vernov and Chudukov [1960] independently reported on the existence of very energetic particles trapped in the geomagnetic field in near-Earth space. The particle intensities exhibited a two-zone structure, with two local maxima around L ~1.5 and L ~4. The L-parameter [McIlwain, 1961] is defined for any magnetic field line as the radial distance from the center of the Earth to the intersection of the field line with the magnetic equatorial plane; it is useful for radiation belt physics since it can approximately map observations at any latitude to a radial distance in Earth radii (R_E) at equatorial latitudes. Due to the nature of charged particle motion in Earth's dipole-like magnetic field, trapped energetic particles (i.e., those that are relatively immune to effects from the corotational or convective electric fields) undergo three characteristic motions: gyration around field lines, bounce between mirror points along field lines, and azimuthal drift around Earth. Due to these motions the zones of ionizing radiation are toroidal in shape, circumscribing the planet, which led to their being referred to as radiation belts. Each of the three characteristic motions of radiation belt particles can be related to an adiabatic invariant, μ, K, and Φ (or L^*, the invariant L-parameter). For detailed discussions of the motion of radiation belt particles and the adiabatic invariants, see Northrop and Teller [1960], Roederer [1970], Schulz and Lanzerotti [1974], and more recently Green and Kivelson [2004] and Ukhorskiy and Sitnov [2012].

As spacecraft launched throughout the 1960s provided more and more observational evidence, scientists developed a better understanding of radiation belt climatology [e.g., Van Allen, 1969; Vernov et al., 1969]. The inner belt consisting of both protons and electrons is relatively stable compared to the outer belt, consisting of electrons ranging in energy from hundreds of keV to several MeV, which exhibits extreme variability in intensity over a range of timescales. It was recognized early that magnetically disturbed periods, and in particular geomagnetic storms, result in drastic variations of the intensity of outer radiation belt electrons. Sudden inward shifts of the entire outer belt distribution are observed immediately following many storm sudden commencements [e.g., Vernov, 1968]. During storm main phase, the intensity of >150 keV electrons decreases abruptly [e.g., McIlwain, 1966a], but the intensity of electrons at lower energy (E > 40 keV) does not always reveal a similar decrease [e.g., Craven, 1966]. However, during the recovery phase of storms (i.e., after the minimum in the Dst index), rapid enhancements of outer belt electron intensities were often reported. The enhancement timescale is delayed based on electron energy: for E > 40 keV electrons, timescales of <3 hours were reported by Craven [1966], while for E > 150 keV, the enhancement time was longer, around ~12–36 hours [Vernov et al., 1966]. Drastic electron enhancements during recovery phases were also observed at higher energies, >240 keV to >1 MeV [e.g., Williams et al., 1968] and even >5 MeV [McIlwain, 1966b].

Russell and Thorne [1970] also showed how the "slot" region between the inner and outer electron belts could be partially filled during periods of enhanced geomagnetic activity.

Various theories were developed to explain the observations of outer radiation belt dynamics. Vernov [1968] described the inward displacement of the belt at the beginning of many storms as rapid radial diffusion, an irreversible process. Depletions during the main phase, referred to as flux dropouts [see review by Turner et al., 2012a], were explained by Dessler and Karplus [1961] as resulting from adiabatic radial transport of trapped energetic particles due to the strong variations in the global magnetic field during geomagnetic storms. Enhancements of the outer belt during geomagnetically active periods were initially thought to result from enhanced inward radial diffusion from a source of electrons in the plasma sheet, though as we'll see later, this isn't the full story. Radial diffusion theory in Earth's radiation belts, along with the formulation for momentum and pitch angle diffusion, was presented in great detail by Schulz and Lanzerotti [1974].

Wave-particle interactions are critical to quasilinear diffusion theory, as these provide the random or resonant energy kicks to the particles, breaking one or more of the adiabatic invariants and enabling diffusion of the particle distributions. Quasilinear theory proved very successful as a model to explain the radiation belts. For example, Lyons and Thorne [1973] explained a steady state of the electron radiation belts using a combination of inward radial diffusion from a source population at L = 5.5 and losses due to Coulomb scattering at very low L-shells and pitch angle diffusion throughout the plasmasphere. In the model, inward radial diffusion from the boundary condition at L = 5.5 provided a source of electrons, while the losses ultimately resulted in the formation of the slot region. This picture of the electron radiation belts—in which a source of electrons at high L-shells was accelerated by conservation of μ and K as they diffused radially inward to regions of higher magnetic field strength—was widely accepted. In this picture, storm-time depletions were dominated by adiabatic and entirely reversible variations due to variations in the global magnetic field, and true losses resulted primarily from pitch angle diffusion into the atmospheric loss cone. The strong variations observed in the belt during geomagnetically active periods were thought to simply be a result of strong variations in the diffusion coefficients due to enhanced wave activity.

This picture of the radiation belts remained *mostly* unchallenged [for some exceptions see: Baker et al., 1989; Fujimoto et al., 1990] until the early 1990s, after the launch of the Combined Release and Radiation Effects Satellite (CRRES) and Solar, Anomalous, and Magnetospheric Particle Explorer (SAMPEX) missions. CRRES was launched on July 25, 1990, into a geosynchronous transfer orbit (period ~10 hours) with an inclination of 18°. This orbit, combined with its suite of particle, fields, and waves instrumentation, made CRRES ideal for studying Earth's radiation belts [e.g., Meredith et al., 2003]. SAMPEX was launched on July 3, 1992, into a high inclination low-Earth orbit; it carried a suite of energetic particle telescopes, which allowed for observations of trapped and precipitating electrons from the outer radiation belt.

Observations from these spacecraft [e.g., Blake et al., 1992; Baker et al., 1994; Li et al., 1997] and the subsequently launched Polar spacecraft [Blake et al., 1995; Selesnick and Blake, 1997] quickly demonstrated that the extreme variations in the outer radiation belt involved more complex processes than were fully appreciated previously.

In the post-CRRES era, the newfound appreciation for the complexity of outer radiation belt dynamics has led us to where we are today. Understanding outer belt variability is becoming increasingly important as human society becomes more dependent on space-based assets, to which relativistic electrons in the outer belt pose a threat. With existing missions such as NASA's THEMIS and NOAA's GOES and POES plus the recently launched NASA Van Allen Probes, and NSF's FIREBIRD and Colorado Student Space Weather Experiment (CSSWE) CubeSats, we now have a sizeable fleet of spacecraft available to study Earth's outer belt electrons. This paper is meant to provide a primarily observational overview of our current understanding of the drivers of extreme variations in the intensity of relativistic electrons in Earth's outer radiation belt. The paper is structured as follows: The next section discusses key observations and theory since the launch of CRRES and leading up to the current era (i.e., up to 2007). The third section presents some example cases from the current era, in which (with the advent of NASA's five-satellite THEMIS mission) multi-spacecraft analysis from a near-equatorial vantage point, together with increasingly well-instrumented NOAA geosynchronous and polar orbiting satellites, has provided an unprecedented understanding of the underlying mechanisms responsible for drastic and sudden enhancements, depletions, and transport of outer belt electrons. Note that here we do not focus specifically on storm-time variations, though many of the cases of extreme variability occurred during geomagnetic storms. For a detailed overview of the behavior of the radiation belts and ring current during geomagnetic storms, please see Reeves and Daglis [this volume]. We finish with a section outlining several of the many outstanding questions and topics of future research concerning outer belt variability followed by a brief conclusion and summary.

12.2 Physical processes that can drive extreme outer belt variability

It has long been appreciated that the intensities of relativistic electrons in Earth's outer radiation belt fluctuate by orders of magnitude over a range of timescales, from minutes to decades [e.g., see reviews by Li and Temerin, 2001; Friedel et al., 2002; and Millan and Baker, 2012]. Outer belt variations are ultimately driven by fluctuations in various solar wind parameters, but that relationship is complex and relies on many internal processes within the magnetosphere, each of which is also related to activity in the solar wind [e.g., Hudson et al., 2008]. Figure 12.1 shows an example of this variability in observations from NASA's THEMIS mission [Angelopoulos, 2008]. Each THEMIS spacecraft passes through the entire outer radiation belt twice per day very close to the

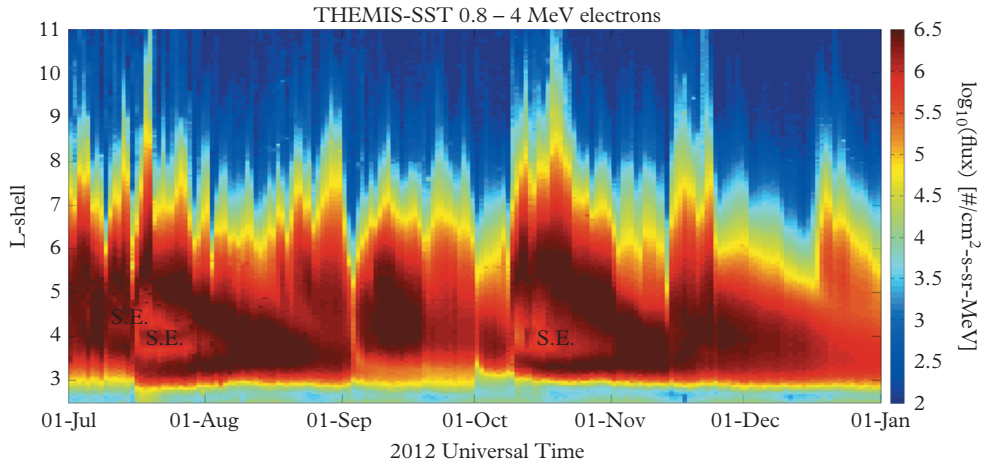

Figure 12.1 *Relativistic electron fluxes from the highest channel (0.8 to ~4 MeV) on the THEMIS Solid State Telescope (SST) instruments binned and averaged by time (daily) and L-shell ($\Delta L = 0.05$). Data are combined from all three THEMIS spacecraft (THA, THD, and THE) from July 1 to December 31, 2012. Log_{10} of flux is shown in color. The instruments sometimes suffer from saturation in the heart of the outer belt during periods in which the electron fluxes are very enhanced; such regions on the plot are marked with S.E. for "saturation effect."*

magnetic equator. The Solid State Telescopes (SSTs) on board each THEMIS satellite provide energy and pitch angle resolved fluxes of energetic ions and electrons from ~30 keV to several MeV [e.g., Turner et al., 2012b]. Figure 12.1 shows daily averaged, 0.8–4 MeV electron fluxes compiled from the SST instruments on the three THEMIS spacecraft still remaining in Earth orbit (THA, THD, and THE; THB and THC became the ARTEMIS mission in 2011) from July 1, 2012, to December 3, 2012. This period showcases how the intensity within the belt, as well as at its outer boundary can vary by more than two orders of magnitude from day to day. Rapid enhancements are visible on days like July 16, October 9 (both of which resulted in the SST instruments saturating in the heart of the outer belt), and November 14, while dropout events can be clearly seen on days like September 3 and October 1. Several of the example events that we discuss in the next section occurred during this period, as did the launch of the Van Allen Probes mission (formerly Radiation Belt Storm Probes [Mauk et al., 2012]). In this section, we present the background theory and supporting evidence of the various source, loss, and transport processes that have been identified as important to driving some of the most extreme cases of outer belt variability.

12.2.1 Sources

Understanding source processes is fundamental to understanding rapid outer belt enhancements. Reeves et al. [1998] and Li et al. [1998] examined an enhancement

of outer radiation belt electrons that occurred on January 10–11, 1997. During this event, spacecraft at geosynchronous orbit (GEO) observed the fluxes of relativistic electrons increasing by more than two orders of magnitude in only around 12 hours. The enhancement was triggered by the impact of an interplanetary coronal mass ejection (ICME). The ICME in question included a period of strong, steady southward B_Z in the interplanetary magnetic field (IMF); during this period, there was strong substorm activity including rapid fluctuations of the energetic particles observed at GEO. Based on the observations, Reeves et al. [1998] concluded that the source of >2 MeV electrons was located inside of GEO during the enhancement event. Li et al. [1998] concluded that the source was the result of enhanced substorm injections introducing a seed population that was subsequently energized by the electromagnetic pulse attending the passage of the ICME shock. Both explanations contradicted the old picture of acceleration by inward radial diffusion from a source in the plasma sheet.

Around the same time, a different theoretical framework was developed to explain the source of relativistic electrons in the heart of the outer radiation belt. Following conceptual work on the topic by Temerin et al. [1994], Summers et al. [1998], and Horne and Thorne [1998] presented a theory of local acceleration of electrons from a seed population of from tens to hundreds of keV to relativistic energies via wave-particle interactions with whistler-mode chorus waves. In this framework, electrons interact with chorus waves [e.g., Li et al., 2009 and references therein] via Doppler-shifted cyclotron resonance, resulting in energy diffusion. Provided many such interactions as electrons drift around the Earth, individual electrons could be stochastically accelerated up to relativistic energies. Horne et al. [2005] showed that acceleration timescales for seed electrons (tens to a few hundreds keV) to be accelerated to ~MeV energies via interactions with chorus waves should be around 1–2 days. Such a scenario is depicted in the conceptual schematics in Figure 12.2.

One key to distinguishing between source mechanisms was to convert electron flux observations to phase space density (PSD) as a function of the adiabatic invariants (μ, K, and L^*), since such a conversion effectively removes purely adiabatic variations from the data. By examining the radial distributions (i.e., in L^*) of electron PSD for fixed values of μ (analogous to energy) and K (analogous to pitch angle), it was possible to look for telltale signatures of the source location of outer radiation belt electrons. This is summarized on the right-most plots in Figure 12.2a: electrons with a source in Earth's plasma sheet should have a maximum in the PSD radial distributions in the plasma sheet itself (i.e., at high L-shells), whereas electrons that are locally accelerated within the heart of the outer belt should have radial profiles that are peaked, with the peak being collocated with the waves that are causing the acceleration. For a more detailed discussion on this, see Green and Kivelson [2004] and/or Reeves et al. [2013].

As observations of the outer radiation belt improved, much evidence in favor of an internal source of relativistic electrons has appeared in the literature. Meredith et al. [2003] showed statistical results from CRRES that outer belt enhancement events occur just outside of the plasmapause during periods of prolonged substorm activity and enhanced

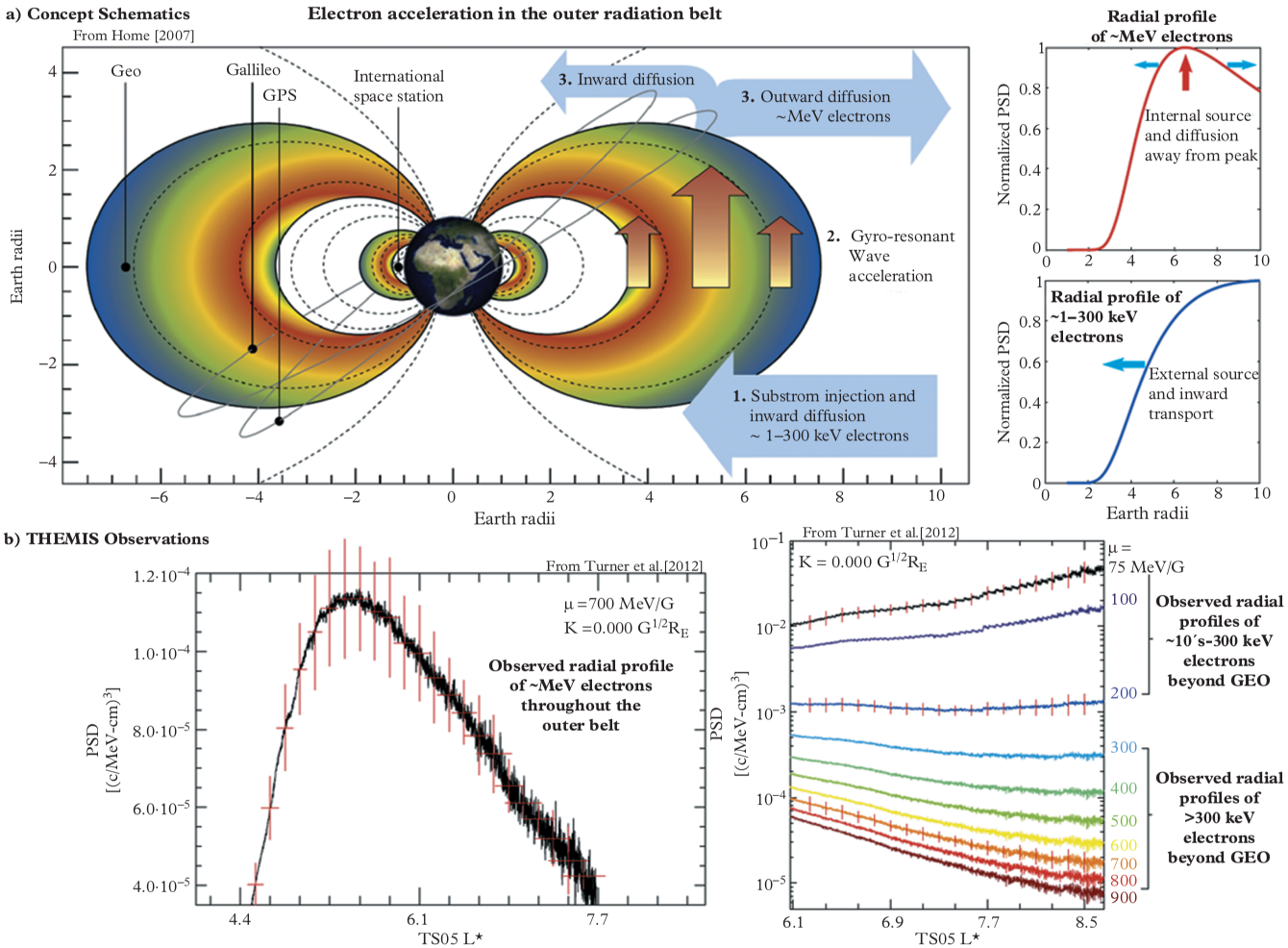
a) Concept Schematics
Electron acceleration in the outer radiation belt
From Home [2007]
Geo
Gallileo
GPS
International space station
3. Inward diffusion
3. Outward diffusion ~MeV electrons
2. Gyro-resonant Wave acceleration
1. Substrom injection and inward diffusion ~ 1–300 keV electrons
Earth radii
Earth radii
Radial profile of ~MeV electrons
Normalized PSD
Internal source and diffusion away from peak
Radial profile of ~1–300 keV electrons
External source and inward transport
Earth radii
b) THEMIS Observations
From Turner et al.[2012]
μ =700 MeV/G
K =0.000 G^1/2R_E
Observed radial profile of ~MeV electrons throughout the outer belt
PSD [(c/MeV-cm)^3]
TS05 L*
From Turner et al.[2012]
K = 0.000 G^1/2R_E
μ = 75 MeV/G
100
200
300
400
500
600
700
800
900
Observed radial profiles of ~10´s-300 keV electrons beyond GEO
Observed radial profiles of >300 keV electrons beyond GEO
PSD [(c/MeV-cm)^3]
TS05 L*

Figure 12.2 *Comparing the conceptual scenario of energy-dependent sources of radiation belt electrons to observations from THEMIS. (a) Schematic from Horne [2007] (top left) showing how ~1 to 300 keV electrons can be injected due to substorm activity (or enhanced convection) and inward radial diffusion. These electrons serve as the source population of chorus waves and the seed population that can be accelerated to >1 MeV by gyro-resonant wave-particle interactions with the chorus. This local acceleration results in a peak in the phase space density (PSD) profile around the radial distance (L-shell) of the wave-particle interactions, and—provided the third invariant is broken by wave activity—the PSD can diffuse away from this peak. Schematics at the top right show the PSD radial distributions in the equatorial plane for the scenario described above. The lower energy, ~1–300 keV electrons (bottom right of the three plots in (a)) have a source population, and thus a maxima in PSD, in the near-Earth plasma sheet, while the relativistic electrons (top right of the three plots in (a)) have a local source population within the heart of the outer belt. (b) Both plots from Turner et al. [2012b]: THEMIS observations are consistent with the above scenario. The left plot in (b) shows the PSD versus L^* of relativistic, equatorially mirroring electrons, which reveals a peak at around L^* ~5.5. The right plot in (b) shows the PSD versus L^* over a broader range in μ (and energy) as the THEMIS spacecraft move beyond geosynchronous orbit into the near Earth plasma sheet. The outward gradients are positive for lower-energy electrons, indicating a source in the plasma sheet, but negative for relativistic electrons, indicating a source inside of GEO. Turner et al. [2012b] showed that these μ-dependent radial distributions are typical for outer belt electrons.*

chorus waves. Observational studies examining PSD of outer belt electrons at fixed values of μ and K have mostly indicated that, for relativistic electrons above ~500 keV in the heart of the outer belt, the PSD profiles in L^* are most often peaked [e.g., Green and Kivelson, 2004; Chen et al., 2007; Turner et al., 2010, 2012b; Kim et al., 2010; Shprits et al., 2012]. In fact, the results presented by Turner et al. [2012b] proved remarkably consistent with the theory of local acceleration via wave-particle interactions with chorus waves. These results are summarized in Figure 12.2b, which shows THEMIS observations of electron PSD for fixed invariants. Positive radial gradients beyond GEO for electrons with energies of ~80 to ~300 keV energy in the heart of the belt indicate a source in the plasma sheet, while negative gradients beyond GEO and peaked distributions for relativistic electrons indicate a source in the inner magnetosphere, within the heart of the outer belt. Modeling efforts [e.g., Shprits et al., 2006a; Su et al., 2011; see also review by Shprits et al., 2008b] have proven successful at capturing rapid enhancements (i.e., ~2 orders of magnitude or more increase in only ~1 day) via local acceleration of electrons by whistler-mode chorus, but observationally the question remained as to whether this mechanism was able to rapidly enhance the entire outer belt of relativistic electrons in only ~1/2 day. In the next section, we examine some example cases during the THEMIS and Van Allen Probes eras that can be used to address this question.

Kataoka and Miyoshi [2008] showed that during solar cycle 23, the strongest enhancements of MeV electrons at GEO were associated with rarefaction periods of very low solar wind density and high, but declining, solar wind speed during the end of geomagnetically active periods. They concluded that such enhancements are the result of

both enhanced source mechanisms *and* reduced loss mechanisms. This underlines the fact that ultimately outer belt variations result from sources dominating over losses or vice versa, and next, we also outline our current understanding of mechanisms that can result in sudden losses of outer belt electrons.

12.2.2 Losses

Being responsible for extreme depletions of the outer radiation belt, losses of relativistic electrons also play a critical role in outer belt variability. Ultimately, loss of outer belt electrons occurs due to: escape via the inner boundary (i.e., precipitation into Earth's atmosphere), escape via the outer boundary (i.e., through the magnetopause), and deceleration, which can possibly occur due to nonlinear wave-particle interactions [e.g., Bortnik et al., 2008] or outward radial transport (e.g., outward diffusion in L^*) [see review on losses by Millan and Thorne, 2007]. Pitch angle diffusion and rapid scattering of outer belt electrons into the atmospheric loss cone can occur due to wave-particle interactions with various plasma waves, such as plasmaspheric hiss [e.g., Thorne et al., 2013a], chorus [e.g., Shprits et al., 2007; Tao et al., 2012], and electromagnetic ion cyclotron (EMIC) waves [e.g., Albert, 2003; Ukhorskiy et al., 2010]. The diffusion coefficients, and thus effective loss rates, for different waves interacting with radiation belt electrons are dependent on electron energy, pitch angle, and location [e.g., Shprits et al., 2008b]. In contrast, losses through the magnetopause are relatively independent of electron energy, though there is some dependence on pitch angle due to drift-shell splitting [e.g., Kim et al., 2008]. Magnetopause shadowing is a term describing the sudden loss of electrons due to sudden inward motion of the magnetopause, which effectively empties previously closed drift shells of electrons within one drift period [e.g., Desorgher et al., 2000; Kim et al., 2010]. Finally, non-adiabatic outward radial transport, such as radial diffusion [e.g., see review by Shprits et al., 2008a], results in electrons becoming irreversibly decelerated as they move to regions of weaker magnetic field strength and longer field lines while conserving μ and K.

Flux dropouts are a good example of extreme variability of the outer radiation belt electrons. Since Li et al. [1997] and Kim and Chan [1997], it has been appreciated that adiabatic effects (i.e., the "Dst effect") alone cannot explain all of the flux variation observed during many radiation belt flux dropout events, and several of the loss mechanisms introduced above have been used to explain the sudden losses of electrons throughout the outer belt during dropouts. The two leading theories are loss to the atmosphere due to wave-particle interactions with EMIC waves [e.g., Thorne et al., 2006] and loss due to magnetopause shadowing and subsequent enhanced outward radial transport [e.g., Shprits et al., 2006b]. There has been observational evidence in favor of both mechanisms: Green et al. [2004], O'Brien et al. [2004], Selesnick [2006], Borovsky and Denton [2009], and Ukhorskiy et al. [2010] all concluded that atmospheric losses could explain dropouts; Horne et al. [2009], Loto'aniu et al. [2010], Morley et al. [2010], Matsumura et al. [2011], Meredith et al. [2011], Shprits et al. [2012], and Turner et al. [2012c] all showed results in favor of magnetopause shadowing and

outward radial transport; meanwhile Bortnik et al. [2006] concluded that losses to the outer boundary dominated at higher L-shells (>∼5) but atmospheric losses dominated at lower L-shells. For full details plus additional references, see the review on outer belt dropouts by Turner et al. [2012a], which concluded that *most*, but not all, dropouts are more consistent with the theory of magnetopause shadowing and outward radial transport.

When the magnetopause is suddenly compressed by an enhancement of solar wind dynamic pressure, electrons on previously closed drift shells may suddenly escape through the magnetopause within only one drift period. This results in a very distinct radial distribution of electrons in the outer radiation belt: a very sharp gradient remains in the distribution at the drift shell that maps to the innermost magnetopause distance. Provided sufficient wave activity to invalidate the third adiabatic invariant and allow for particle transport across drift shells (i.e., in L^*), a cascade or spillover effect will occur, in which the many more electrons at lower L-shells that are transported to higher L-shells are not fully replaced by the very few electrons at higher L-shells that get transported to lower L-shells. This process is compounded by radial diffusion being much more effective at higher L-shells [e.g., Brautigam and Albert, 2000; Selesnick and Blake, 2000] and how electrons lose energy as they move outward in the geomagnetic field. The wave activity required for the radial transport may be manifested as enhanced ULF wave activity resulting from the variations in the solar wind that caused the magnetopause motion [e.g., Turner et al., 2012c].

An example of the effect of magnetopause shadowing and outward radial transport on a distribution of electrons in the outer belt is illustrated with the simulation results shown in Figure 12.3d. This simulation solved the one-dimensional radial diffusion equation [e.g., Shprits et al., 2008a] for a dropout event that occurred on September 30, 2012. The initial condition was based on THEMIS observations of electron PSD at μ = 750 MeV/G and K = 0 $G^{1/2}R_E$ distributed in L^* throughout the belt prior to the dropout. The inner boundary, and L^* = 1 was held at zero PSD, while the outer boundary condition changed in time to simulate the effects of magnetopause shadowing. As seen in Figure 12.3a, there were two sudden enhancements of solar wind dynamic pressure shortly after 11:00 UT and 23:00 UT on September 30. These resulted in sudden inward motion of the magnetopause and a reduction in the last closed drift shell (i.e., L^*_{max} in Figure 12.3c). To simulate the effect of magnetopause shadowing, the PSD at all drift shells affected by the two magnetospheric compressions were reduced to 1% of the peak value from the initial condition, which is again consistent with observations from THEMIS during the dropout. These losses were added at the beginning of the simulation and then 12 hours after, just as was observed. To compare with the THEMIS observations of the pre-to-post-dropout distributions (discussed further in the next section), the simulation was run for 19 hours using an L^*-dependent diffusion coefficient (D_{LL}) based on that used by Selesnick and Blake [2000], which is representative of active conditions (see Figure 12.3d for the equation used here). This simulation shows the effect of the two magnetopause shadowing events on the outer belt. Note that the loss of PSD extends into lower L^* than the innermost extent of the magnetopause shadowing

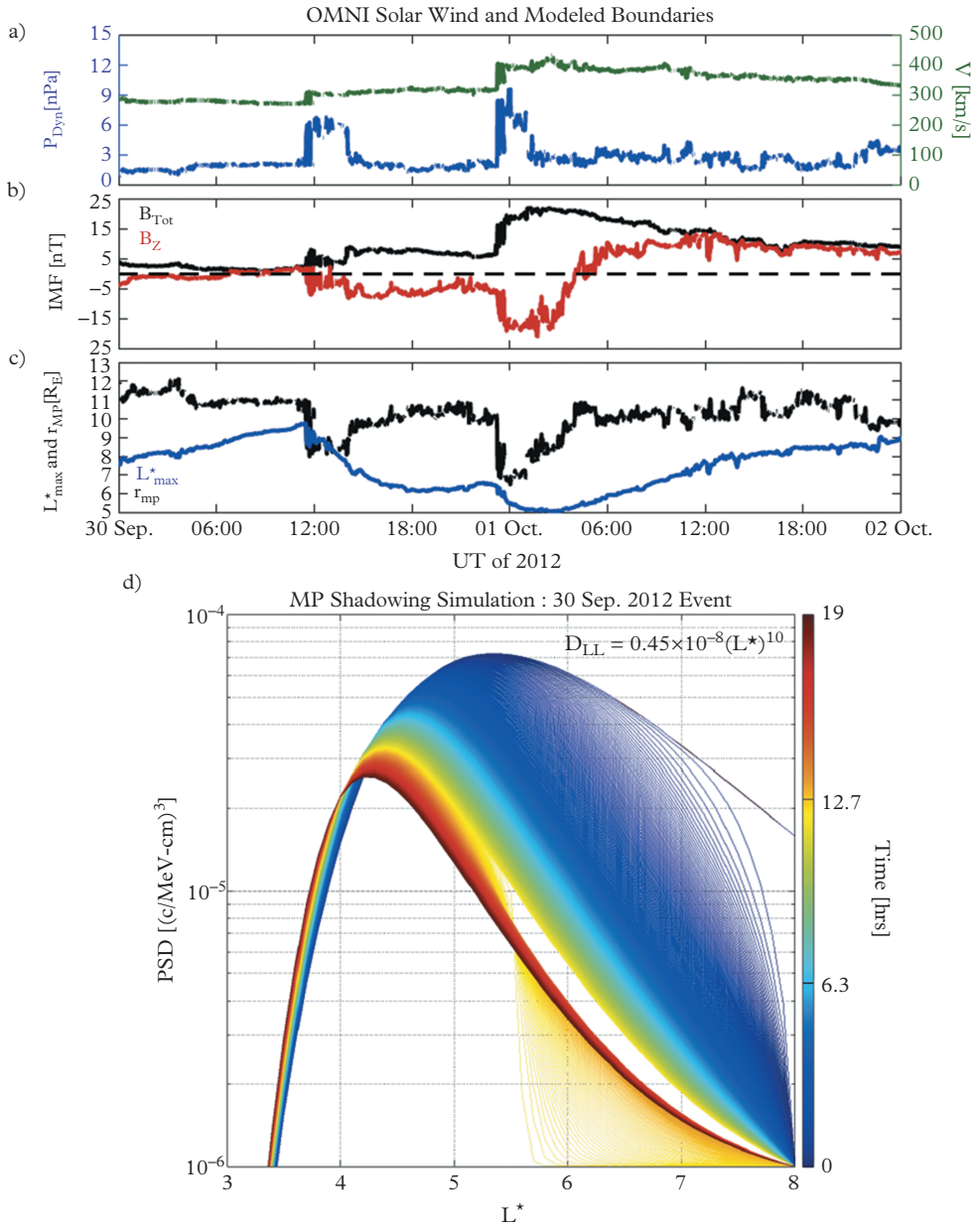

Figure 12.3 *(a), (b), and (c) From Turner et al. [2013b] OMNI solar wind dynamic pressure and speed (a), IMF strength and Z_{GSE} component (b), and the magnetopause standoff distance and last closed drift shell,* L^*_{max} *(c) all from the September 30, 2012, dropout period. (d) One-dimensional radial diffusion simulation results of the PSD evolution as observed by THEMIS during the dropout. See text for details.*

itself (i.e., L^* ~8 and ~5.5 for the two compressions, respectively); this is because of the rapid outward radial diffusion that occurs across the sharp radial gradients in the PSD radial distribution remaining after each instance of shadowing. The simulation shows how the peak in PSD moves down in amplitude and in to lower L^*, with losses at all $L^* > \sim 4$, in less than a day. The loss in PSD is strongest at higher L^*. Also, note that at lower L^*, there is actually an increase in PSD due to inward radial diffusion. Finally, this mechanism should act relatively independent of particle energy and species. These are all key signatures of this mechanism, which we will discuss further in the next section.

Magnetopause shadowing can explain ~88% of outer belt dropout events [e.g., Shprits et al., 2012]. Wave-particle interactions resulting in losses to the atmosphere may still play an important role in those other 12% of cases. Indeed, relativistic electron precipitation into the atmosphere is observed [e.g., Millan et al., 2010], and estimates of the loss rate as a percent of the total trapped population [e.g., Tu et al., 2010] are improving rapidly with increased data availability from LEO spacecraft [Li et al., 2013]. Furthermore, losses into the atmosphere likely play just as important a role as weak sources during prolonged depletion periods of the outer belt electrons, such as occurred through much of 2009 (more details on this period in the next section).

12.2.3 Transport

Radial transport processes can also result in extreme variations of the outer radiation belt electrons. In the previous section, we described how rapid outward radial transport could play a role in outer belt dropout events. Rapid transport can also lead to sudden flux enhancements of radiation belt electrons. Li et al. [1998] presented observations of injections of electrons in the outer radiation belt due to two different processes: substorms and magnetospheric impacts from interplanetary shocks. Starting with the latter, when an interplanetary shock impacts the magnetosphere, a compressional fast mode wave is launched near the subsolar point and propagates tailward. Using a simple wave model based on CRRES observations from the shock impact on March 24, 1991, Li et al. [1993] performed test-particle simulations of radiation belt electrons to examine how they would react to the shock impact. Their simulations showed how electrons are transported radially inward when they interact with the fast magnetosonic wave. The results successfully reproduced the CRRES observations of multi-MeV electrons that were injected into $L < 3$ following the shock impact, as was initially reported by Blake et al. [1992]. This injection formed a new radiation belt in the slot region in only around a minute. The Halloween storms of 2003 [e.g., Baker et al., 2004; Shprits et al., 2006a] also included the sudden formation of a new radiation belt within the slot region due to an injection from the impact of a CME shock in the solar wind. Once injected to such low L-shells, the multi-MeV electrons can remain for over a year after, as seen in Figure 12.4 (from Figure 1 of Baker et al. [2004]). Shock injections transport particles radially inward throughout the outer belt, which can be used to determine the PSD radial gradient just prior to the injection [Li et al., 2003a; Turner and Li, 2008; Kim et al., 2010; Turner

et al., 2010], and since the particles conserve μ and K, they are also energized by the injection. Thus, shock injections are an acceleration mechanism that can result in very sudden enhancements of outer radiation belt electrons.

Energetic particles can also be suddenly injected into the inner magnetosphere during active periods related to dipolarization events and substorms [e.g., Birn et al., 1997, 1998]. Li et al. [1997, 2003b] successfully simulated energetic (tens of keV up to ~300 keV) electron injection signatures and drift echoes at GEO using a model consisting of a transient azimuthal (i.e., cross-tail) electric field signature associated with an increase in B_z, both near-Earth features of substorm dipolarization. Gabrielse et al. [2012] used typical, earthward-traveling, azimuthally localized electric field features of dipolarization fronts [e.g., Runov et al., 2011; Liu et al. 2013] and a guiding center test-particle model constrained by THEMIS multipoint observations to model energetic particle injections. With that model, they were able to explain many of the features typically observed during particle injections not only at but also beyond GEO. For example, they showed how flux depletions observed at some energies during injections can result from return flows at the edges of the fast flow channels that make up the earthward injection.

Concerning extreme cases, Ingraham et al. [2001] reported an unusual case in which an energetic electron injection observed at GEO included relativistic electrons with energy exceeding 1 MeV. This upper energy threshold was much higher than what is typically observed (i.e., a few hundred keV). The injection occurred in the recovery phase of the March 24, 1991, storm during a period of intense substorm activity. These observations showed a clear increase in the upper energy threshold of injected electrons as the ambient population of relativistic electrons also increased in the rapid and drastic outer belt enhancement event that occurred during the recovery phase of that storm. The Ingraham et al. [2001] results provide additional evidence of the importance of substorm-injected electrons during outer belt enhancement events.

Radial transport may also be relatively chaotic at high L-shells on the dayside of the magnetosphere. Due to the compression of the dayside magnetic field, the location of minimum magnetic field strength along field lines at higher L-shells (typically beyond GEO) actually moves away from the magnetic equator to higher latitudes. When trapped radiation belt electrons encounter such regions, their drift shells bifurcate, and some of them, depending on their pitch angle and bounce phase, start bouncing around the minimum-B location either above or below the equator. Such bifurcated drift orbits are often referred to as Shabansky orbits after Shabansky [1971]. Ukhorskiy et al. [2011] conducted test particle simulations to study the effects of these bifurcated drift orbits on trapped electrons. They found that some electrons undergo bifurcated drift orbits and get scattered randomly in pitch angle and L-shell. Most of those electrons remained quasi-trapped in the bifurcation region for a long time. Due to the random mixing associated with the chaotic motion, some electrons were accelerated by a net inward radial diffusion, but some electrons were also lost through the magnetopause or into the atmospheric loss cone. McCollough et al. [2012] examined EMIC wave growth due to the effects of ions undergoing bifurcated drift orbits. They found that EMIC waves

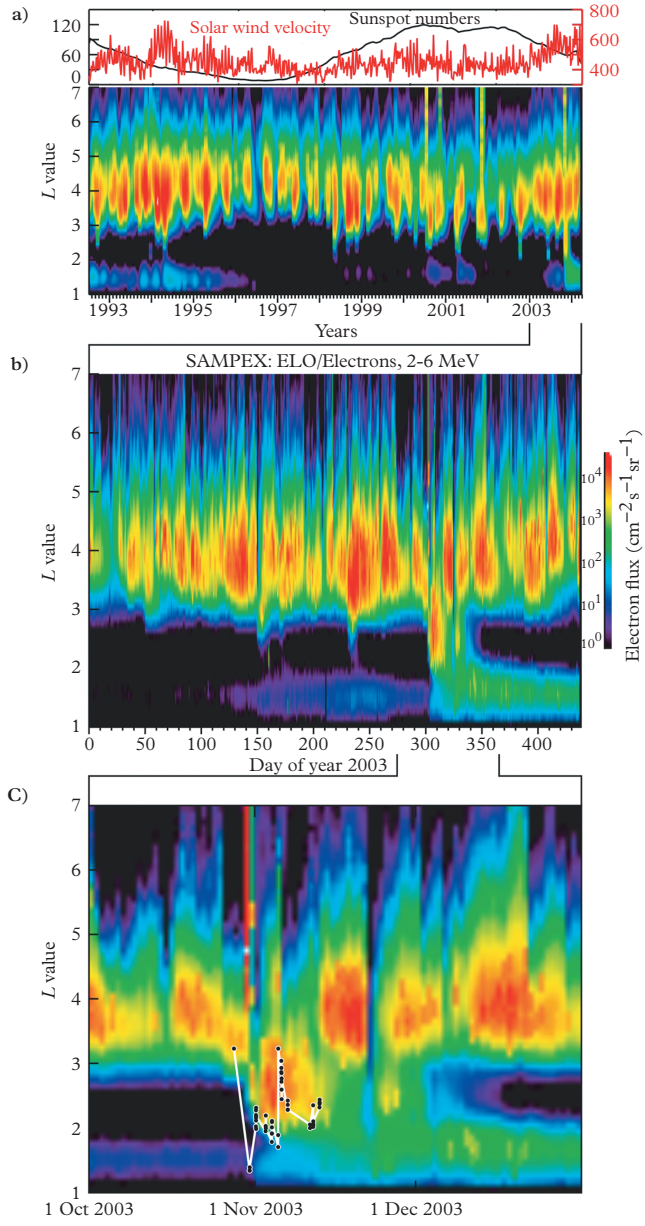

Figure 12.4 *From Baker et al. [2004]: SAMPEX observations of 2–6 MeV electron flux during the entire mission (top-most color plot), 2003 (middle) and around the Halloween 2003 storms (bottom). Flux is binned and averaged in time and L-shell and shown in color. The top plot shows averaged solar wind speed (red) and sunspot number (black) over the course of the SAMPEX mission.*

may be generated in off-equatorial minimum-B pockets on the dayside, which may explain recent observations of bidirectional EMIC waves observed at high L-shells and mid-latitudes on the dayside [Allen et al., 2013] and may also contribute to additional relativistic electron loss at high L-shells.

12.3 Recent multipoint observational examples of extreme outer belt variability

In this section, we discuss recent cases in which the mechanisms outlined in the previous section played a role in driving extreme variations of relativistic electrons in the outer belt. Each case occurred after the launch of NASA's THEMIS mission in 2007, thus allowing for multipoint observations throughout the magnetosphere.

12.3.1 Outer belt enhancements

12.3.1.1 Rapid local acceleration

We examine two cases from the recent literature in which the intensity of relativistic electrons enhanced by over two orders of magnitude throughout much of the outer belt in less than a day. The first occurred on February 4, 2011, and was presented by Turner et al. [2013]. The time history of electron PSD observed by THEMIS for $\mu = 1000$ MeV/G and $K < 0.025\ G^{1/2}R_E$ during the event is shown in Figure 12.5. The initial distribution, shown for THD on its outbound pass starting at 04:30 UT on February 5, revealed a weak, peaked distribution leftover after the main phase dropout of this storm. The next distribution, observed by THE on its outbound pass starting only 30 minutes later, revealed how this peak has grown in time. Furthermore, taking advantage of the multipoint nature of the THEMIS mission, the simultaneous measurements from these two spacecraft confirm that the distribution is indeed peaked and not just time varying. When THE started its pass through the outer belt, THD was already at higher L^* and the PSD gradient was positive; by the time THE got to $L^* \sim 4.5$, THD was at higher L^* and the PSD gradient was negative. Together, these observations confirm that the PSD distribution was peaked somewhere between $4 < L^* < 4.5$ and that this peak grew over time, a telltale signature of local acceleration.

The outer belt continued to enhance over the next 24 hours, as can be seen from the subsequent PSD distributions observed by THD and THE in Figure 12.5. It should be noted that on the inbound passes (dashed lines), the spacecraft were inbound on the dayside, and due to the extreme compression of the magnetopause, L^* was undefined by the Tsyganenko and Sitnov [2005] model at $L^* > \sim 5.75$ on February 5 and $> \sim 6.5$ on February 6. Since L^* is undefined, we did not plot the PSD at higher radial distances for these distributions in that figure. However, the PSD was still calculated for fixed μ and K at these higher L-shells, which revealed that the PSD distributions were indeed peaked as shown at these times. Thus, over the course of only ~24 hours from February 5 to 6, the PSD of relativistic electrons increased by over two orders of

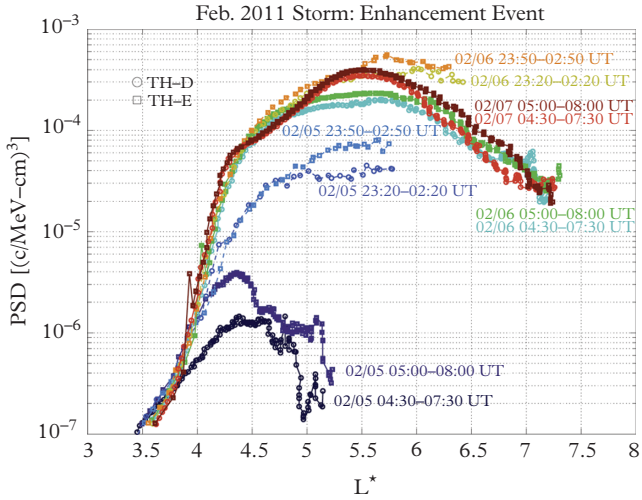

Figure 12.5 *Phase space density distributions from the February 2011 storm. Results from THEMIS-D and -E are shown with circles and squares, respectively. Distributions are color coded by time from February 5 to February 7. The UT ranges shown correspond to the periods that the spacecraft spent in the outer belt for each distribution.*

magnitude at $L^* > 5$ throughout the belt. The time history of the distributions from THEMIS reveals that the PSD was enhanced as growing peaks that started first around $L^* \sim 4.5$ and moved to higher L^* throughout the event. This is strong evidence of local acceleration. Furthermore, Turner et al. [2013] showed THEMIS observations of whistler-mode chorus during the main and recovery phases of this storm; the chorus wave amplitudes were strongest first at lower L-shells during the main and early recovery phases (i.e., $\sim 4 < L^* < \sim 6$ on February 5) and then moved to higher L-shells and covered a broader range over the next day (i.e., $\sim 4.5 < L^* < \sim 7$ on February 6). Chorus activity was not observed on February 7, which coincides with when the peak in PSD stopped growing. Turner et al. [2013] concluded that this event provided strong evidence of rapid enhancement of relativistic outer belt electrons due to local acceleration from wave-particle interactions between seed electrons at tens to hundreds of keV and whistler-mode chorus.

Another very rapid enhancement of relativistic electrons in the outer radiation belt occurred during the October 8–9, 2012, storm. During that event, the fluxes of multi-MeV electrons in the heart of the outer belt increased by over two orders of magnitude in only ~12 hours. Reeves et al. [2013] examined PSD distributions for $\mu = 3433$ MeV/G and $K = 0.11\ G^{1/2}R_E$ through the outer radiation belt from the Van Allen Probes. They found the PSD of these multi-MeV (i.e., "ultrarelativistic") electrons evolved as growing peaks

centered on L^* ~4.3 during the enhancement. Furthermore, they examined PSD derived from THEMIS-SST data in the near-Earth plasma sheet, which revealed negative gradients and thus an insufficient source of these relativistic electrons in the plasma sheet throughout the event. Thorne et al. [2013b] were able to reproduce the enhancement of electrons ranging from hundreds of keV to several MeV using two-dimensional, energy and pitch angle diffusion driven by wave-particle interactions with whistler-mode chorus waves. They modeled the global chorus wave environment using a combination of Van Allen Probes and POES observations. Their results showed that the relativistic electrons could be locally accelerated from a seed population of tens to hundreds of keV electrons by chorus waves, resulting in the more than two orders of magnitude enhancement in only ~12 hours, consistent with observations.

Both events described above revealed growing peaks in PSD for relativistic electrons coincident with enhanced chorus wave activity. Those events occurred during the early recovery phase of geomagnetic storms, consistent with other recent results showing that chorus acceleration should be particularly efficient during the early recovery phase of storms [e.g., Artemyev et al., 2013; Shprits et al., 2013]. However, rapid relativistic electron enhancements need not necessarily be associated with geomagnetic storms. For example, Meredith et al. [2002] presented an outer belt enhancement observed by CRRES during a period of strong substorm activity, and Schiller et al. [2014] presented a case observed by Van Allen Probes and THEMIS in which electrons up to ~1 MeV in the outer belt enhanced by over 2.5 orders of magnitude during a 24-hour period in the absence of a storm (minimum Dst was only ~ –30 nT during a full week around the event). The latter event, however, was also associated with sustained, enhanced substorm activity based on the AL index, further evidence suggesting that enhanced and repeated substorm activity may be an important driver of radiation belt relativistic electron acceleration both during and outside of storms.

12.3.1.2 Shock injections

On St. Patrick's Day (March 17) 2013, an ICME shock impacted Earth's magnetosphere. Despite a gap in the OMNI dataset at the shock impact time, the ARTEMIS spacecraft [Angelopoulos, 2011] were in lunar orbit upstream of Earth's bow shock and observed the ICME and its shock. IMF and solar wind density and velocity observed by ARTEMIS-P2 are shown in Figure 12.6. These observations reveal that the shock hit the spacecraft, in lunar orbit, at around 05:54:30 UT. The Moon was located at ~60 R_E off of the dusk flank at the time. Compared to previously mentioned shocks, such as those associated with the March 1991, and Halloween 2003 events, the St. Patrick's Day shock was relatively weak, with the solar wind density spiking to $< 20\,cm^{-3}$ and speed only jumping to ~650 km/s; the Halloween 2003 events involved a jump in velocity up to approximately 2000 km/s [Li et al., 2009]. Regardless, at the time this paper was written, the St. Patrick's Day event was one of the clearest and strongest interplanetary shocks to impact the magnetosphere during the current solar maximum.

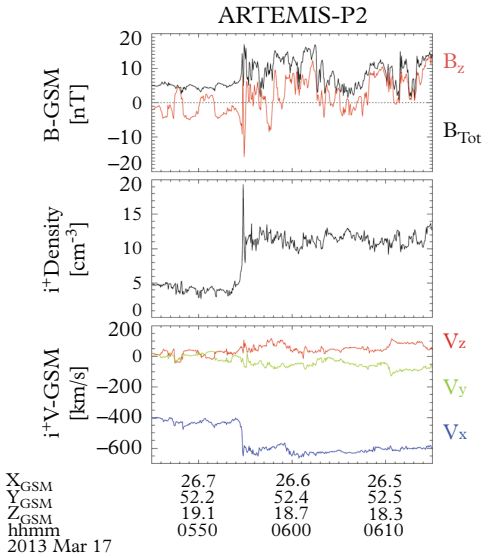

Figure 12.6 *ARTEMIS-P2 observations of the St. Patrick's Day 2013 interplanetary shock at 1 AU. The top plot shows IMF strength (B_{Tot} in black) and Z_{GSM} (B_Z in red). The middle plot shows ion density, and the bottom plot shows ion velocity in GSM coordinates. The spacecraft location is shown along with corresponding UT from March 17, 2013, on the X-axis.*

Using several of the available spacecraft in the magnetosphere, we next examine the effect this shock impact had on energetic electrons in the inner magnetosphere. Figure 12.7 shows THEMIS and GOES magnetic field and energetic electron (tens to hundreds of keV) observations during the same 30-minute period as shown in Figure 12.6. The shock impacted the magnetosphere at ~06:00 UT. At the time of the impact, THA was just outside of GEO and inbound in the noon MLT sector, while THD was also just outside of GEO but was outbound in the dawn MLT sector. THE was inside of 5 R_E at the time, also in the dawn MLT sector, and is not shown here. GOES-13 and -15 were on the night side at around 01:00 and 21:00 MLT, respectively. From Figure 12.7, the shock impact is clearly visible in the magnetic field observations from all four spacecraft. Information of the impact initially moves through the magnetosphere at the fast magnetosonic speed, which only should take a few tens of seconds to traverse the entire inner magnetosphere from the subsolar point to the start of the magnetotail. At 1-minute resolution, the GOES observations cannot resolve the delay time in the arrival of the magnetosonic wave due to its propagation through the system. However, the THEMIS observations clearly reveal this propagation effect: THA observed the compression in the magnetic field first at ~05:59:55 UT, while THE first observed it 18 seconds later at ~06:00:13 UT.

As expected based on previous studies of the effects of shock impacts on radiation belt electrons, all four spacecraft observed clear responses in the tens to hundreds of keV electrons around the time of the impact. Interestingly though, they also revealed some key differences between the different spacecraft. On the dayside near noon, where inward radial transport of electrons in response to the shock impact is most likely [Li et al., 2003a; Turner and Li, 2008], THA observed a slight increase in the flux of electrons at $\leq$ ~200 keV; above this energy, however, THA observed a decrease in

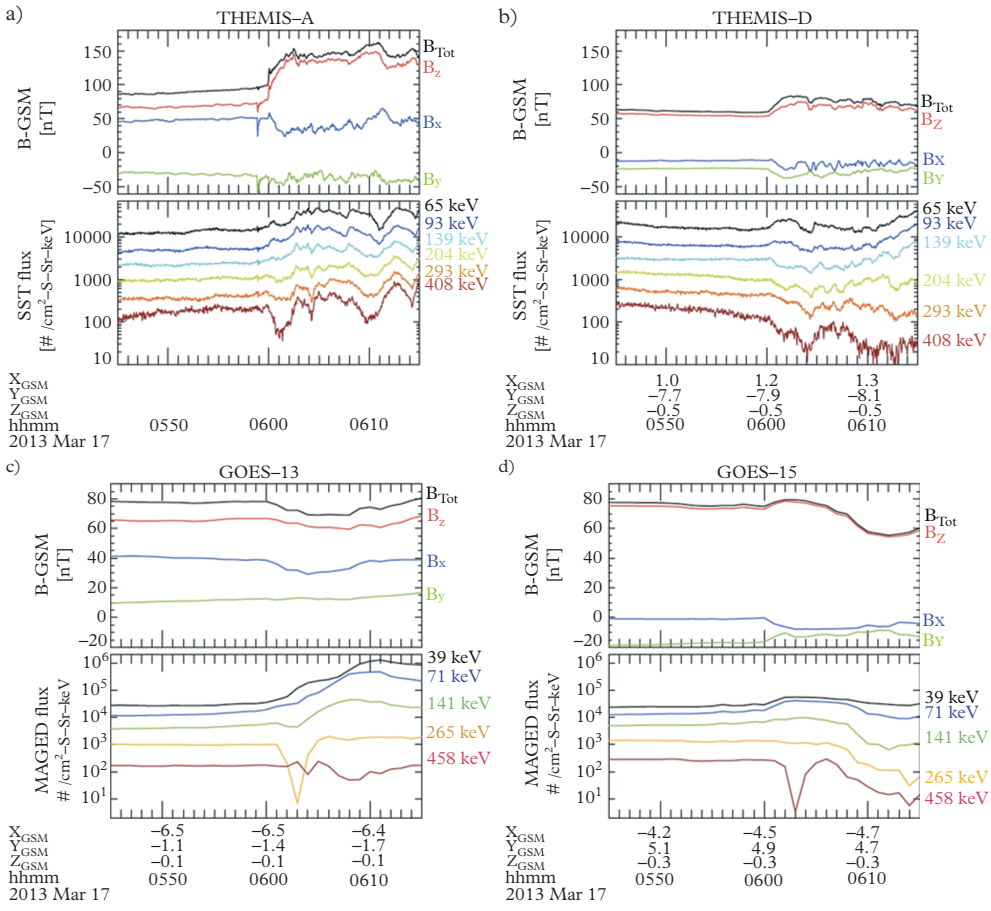

Figure 12.7 *THEMIS and GOES observations from within the magnetosphere during the St. Patrick's Day interplanetary shock impact. For each of the four spacecraft (THEMIS-A and –D and GOES-13 and -15, as labeled above each set of plots), B_{GSM} is shown in the top plot with strength in black and XYZ coordinates in blue, green, and red respectively. Energetic electron fluxes are shown from the SST instruments for THEMIS and the MAGED instruments from GOES with the corresponding energies for each channel shown listed on the right beside each line of data. For all four spacecraft, their locations in GSM coordinates are listed on the X-axis. All four show the same period of time: 05:45–06:15 UT on March 17, 2013.*

fluxes. THD observed similar features, though the transition energy was somewhere between 93 and 139 keV. These energy-dependent responses are typical of shock injections, and they indicate a μ-dependent gradient in the radial distributions of radiation belt electrons [Turner and Li, 2008; Kim et al., 2010; Turner et al., 2010]. The typical transition between positive and negative gradients from previous studies is ∼200

MeV/G (corresponding to ~200 keV at GEO) [Turner et al., 2010, 2012b; see also Figure 12.2b], consistent with the THEMIS results for this event. The response is significantly different at GOES on the night side. While again, the temporal resolution at GOES is too slow to resolve the initial impact propagation delay, we note that the field strength actually decreased at GOES-13 and increased (dipolarized) at GOES-15, while the energetic electrons at both spacecraft exhibited an injection at tens of keV energies at ~06:03 UT and a depletion at one or two channels at hundreds of keV energy. These signatures are consistent with substorm activity triggered by the impact. Localized dipolarization is a hallmark of dipolarizing flux bundles, while the seemingly bizarre flux changes (some increase, some decrease) observed at both GOES spacecraft is similar to events reported by Gabrielse et al. [2012] and explained as due to the spacecraft location in relation to the injection flow channel. Since both spacecraft observed a depletion of higher-energy electrons and there was only a weak dipolarization at GOES-15, neither spacecraft intersected the earthward flow channel.

The St. Patrick's Day event ultimately resulted in an enhancement of the outer radiation belt based on Van Allen Probes data (not shown here) [Baker et al., 2014], with signatures of local acceleration that are remarkably consistent with the scenario in Figure 12.2 [Boyd et al., 2014]. As observed by THEMIS, this event revealed the classic energetic particle signatures associated with injections from an interplanetary shock impact. Furthermore, the GOES observations revealed interesting differences in the response on the night side, as expected based on previous cases [e.g., Li et al., 2003a]. GOES may also have observed one of the first energetic particle injections associated with substorm activity following the impact of the interplanetary shock; as discussed in the previous subsection, injections like this may have played a critical role in the overall enhancement of the belt during the recovery phase of this storm.

12.3.1.3 Energetic particle injections from the plasma sheet

Energetic particle injections from the plasma sheet provide both the source population of several to tens of keV electrons that generate chorus waves and the seed population of tens to hundreds of keV electrons that can be accelerated to relativistic energies (e.g., see Figure 12.2). After a prolonged period of sustained substorm activity, injections of ~MeV electrons at GEO have also been observed [Ingraham et al., 2001], indicating a sufficient source of relativistic electrons at L-shells beyond GEO for that event. For these reasons, it is critically important to understand the nature and characteristics of energetic particle injections.

On July 3, 2012, a fortuitous alignment of the ARTEMIS, THEMIS, Geotail, and GOES spacecraft allowed Angelopoulos et al. [2013] to study in detail the nature of tail reconnection and the results both tailward and Earthward of the reconnection site. The multipoint observations revealed that information of the reconnection travels away from the reconnection site via reconnection fronts of recently reconnected magnetic flux and plasma. These reconnection fronts exhibit significant structure on the electron inertial scales in depth, perpendicular to the local field, which can be responsible for the majority of energy conversion, from magnetic energy stored in the stretched magnetotail to plasma heating, during substorm activity. On the Earthward side of the reconnection

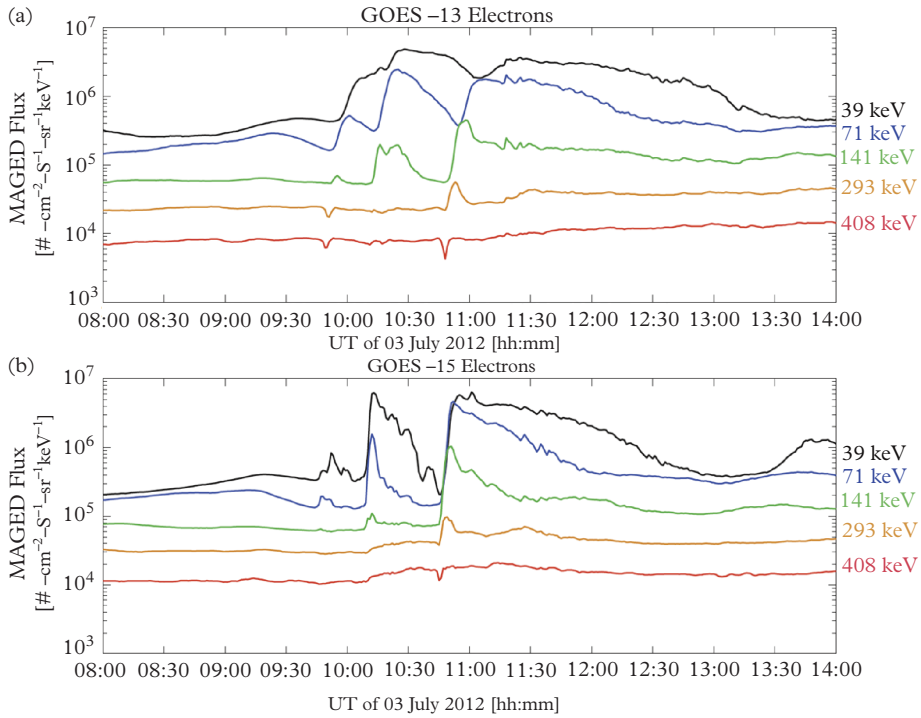

Figure 12.8 *Energetic electron injections observed by GOES-13 (a) and -15 (b) from July 3, 2012. For each satellite, electron flux data from the MAGED instruments are shown from the instruments' five energy channels as listed on the right beside each data line.*

region, these fronts are what have been referred to previously as dipolarization fronts [e.g., Runov et al., 2011]. It is the fields and flow properties around these fronts that are responsible for the rapid inward transport of energetic particles that can manifest themselves as energetic particle injections observed in the inner magnetosphere. For example, Figure 12.8 shows GOES-13 and -15 observations from July 3, 2012, during the arrival of reconnection fronts at the inner magnetosphere from the reconnection site, located $23R_E$ down the tail. During this period, there were three energetic electron injections, observed at GOES-15 around ~09:45, ~10:09, and ~10:45 UT. These injections correspond directly to reconnection fronts observed earlier in the plasma sheet by THEMIS and ARTEMIS [Angelopoulos et al., 2013]. At GOES-15, at post-midnight, the injections were dispersionless, whereas at GOES-13, near 06:00 MLT the injections were dispersed. The increased dispersion at GOES-13 is simply a result of the energy-dependent drift time as electrons move eastward around the system between GOES-15 and -13.

One interesting feature about this case was how the upper energy threshold on the injected electrons at GEO increased from the first to the third injection. For the first injection, GOES-15 (-13) observed an upper energy limit of 71 keV (141 keV), while for

the second and third injections, this upper limit increased to 141 keV (141 keV) and 293 keV (293 keV), respectively. This indicates that there was some heating or acceleration of hundreds of keV electrons in the plasma sheet between the first and last injections, presumably due to the arrival of additional reconnection fronts; the electromagnetic waves associated with the fronts operate on a seed population of progressively increasing energy and flux. Also of interest are the decreases in flux observed by GOES-13 for 293 and 408 keV during the first injection and by both GOES for 408 keV during the last injection. These decreases may be either due to an insufficient source of these electrons at higher L-shells [e.g., Turner et al., 2012b] or entrapment of high-energy electron drift paths in the return flow of injection flow channels [e.g., Gabrielse et al., 2012]. Interestingly, there was an enhancement of >0.8 MeV electrons in the radiation belt on the same day as these injections (e.g., Figure 12.1). The July 3, 2012, series of energetic particle injections from the plasma sheet provides additional evidence of how sustained substorm activity can result in an increase of the upper energy threshold of injected electrons. This may provide an explanation for the ~MeV injections observed by Ingraham et al. [2001] and presents an interesting topic for future work (see details later).

12.3.2 Outer belt depletions

12.3.2.1 Dropout events

Flux dropout events represent one of the most drastic types of depletions that can occur in the outer radiation belt. Here, we showcase two dropout events presented in the recent literature, which highlight important clues as to the dominant loss mechanisms active during dropouts. On January 6, 2011, a dropout resulted in the sudden loss of relativistic electron flux throughout the outer belt above L ~4. Turner et al. [2012c] examined this event using two GOES spacecraft at GEO, the three THEMIS spacecraft, which observed the dropout throughout the belt along the magnetic equator, and six POES spacecraft, which are spread out over a broad range of MLT at low-Earth orbit (LEO). The dropout was clear in the observations from all eleven available spacecraft. Each POES satellite provides simultaneous measurements of trapped electrons near the edge of the loss cone and atmospheric electrons within the atmospheric loss cone. Taking advantage of this, Turner et al. [2012c] presented evidence that the loss of electrons to the atmosphere during the dropout was insufficient to explain the loss observed throughout the outer belt. Based on THEMIS and GOES data used to calculate PSD for fixed values of the three adiabatic invariants, it was clear that the dropout involved true losses from the system and wasn't simply a result of the "Dst effect." Additional key evidence included: the dropout started immediately after the magnetopause was compressed by the high pressure solar wind in a stream-interaction region; and the global ULF wave activity, which should facilitate enhanced radial transport of outer belt electrons, was enhanced by several orders of magnitude over a broad range of L-shells throughout the outer belt following the impact of the stream-interface region. Based on all of these, Turner et al. [2012c] concluded that the losses must have resulted from magnetopause shadowing and subsequent outward transport.

Since Van Allen Probes launched, the radiation belt science community has been afforded an unprecedented level of temporal, spatial, and energy resolution for observations of relativistic electrons in the outer radiation belt. Taking advantage of the addition of these two new spacecraft to the existing fleet capable of observing the outer belt electrons, Turner et al. [2014] studied a dropout that occurred on September 30, 2012, to fully quantify the energy, pitch angle, and L^* ranges and timescales of electrons affected by the dropout. Like the January 2011 event, the September 30, 2012, dropout started after a sudden compression of the magnetosphere associated with an ICME sheath (Figure 12.3a and b). Also, POES observations revealed insufficient loss of relativistic electrons into the atmosphere throughout the majority of the pre-existing belt ($L > 4$). THEMIS and Van Allen Probes electron fluxes were converted to PSD distributions in L^* for fixed values of μ and K. The results from THEMIS are shown in Figure 12.9a. Consistent with the Van Allen results, the pre-dropout PSD distribution was broadly peaked, with the peak location around L^* of ~5.5. Immediately following the first sudden compression of the magnetosphere, a sharp gradient in the PSD distribution was observed around $6 < L^* < 6.5$, after which, the loss moved to lower L-shells over the next ~19 hours until the distribution shown in red from 06:30 UT in Figure 12.9a was observed by THEMIS. Also of interest, after the second sudden compression of the magnetosphere (see Figure 12.3c), another sharp gradient was observed in the PSD distributions from THEMIS and Van Allen at around $L^* \sim 5.5$.

The observed losses during this dropout were consistent with expectations from magnetopause shadowing and subsequent outward transport, as shown in the data-model comparisons in Figure 12.9b. Figure 12.9b compares the percent change in PSD for $\mu = 750$ MeV/G, $K \sim 0$ $G^{1/2}R_E$ electrons as observed by THEMIS (difference between the September 30, 05:30 and October 1, 06:30 pre- and post-dropout curves in Fig. 12.9a, normalized to the pre-dropout values) and also simulated using the simple radial diffusion model shown in Figure 12.3d (note too that Figures 12.9a and 12.3d are on the same scales). The comparison shows that the simple model captures the nature of the dropout remarkably well, including both the loss up to > 90% of the pre-dropout PSD at $L^* > \sim 4.5$ and the enhancement of PSD due to inward diffusion at $L^* < \sim 4.5$. It is gratifying that such a simplified "toy model" can so accurately simulate the behavior of the outer belt; we interpret the agreement as strong evidence in support of magnetopause shadowing and subsequent outward radial transport being the dominant loss mechanism during this dropout event. Using test-particle simulations in global magnetohydrodynamic fields simulated using the solar wind conditions for this event, Hudson et al. [2014] drew the same conclusions. For this dropout and two others in September and October 2012, they found magnetopause shadowing could explain the dropout throughout the majority of the outer belt with additional losses to the atmosphere occurring at lower L-shells.

The two Van Allen Probes provided a significant amount of additional evidence in support of the loss being dominated at $L^* > \sim 4$ by magnetopause shadowing and outward transport as well as evidence of additional losses from a different mechanism at lower L^*. Turner et al. [2014] showed that the dropout was effective for electrons over a broad range in energy, from only a few hundreds of keV to multi-MeV and over the full

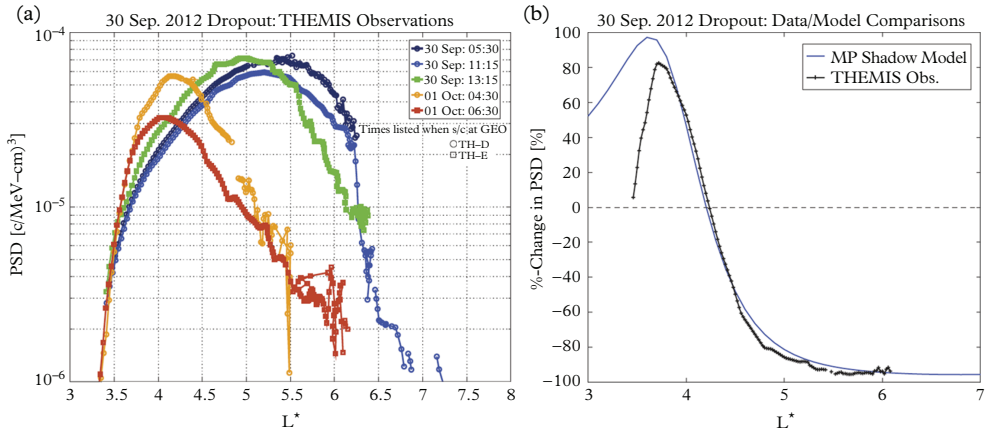

Figure 12.9 *(a) THEMIS observations of the PSD L*-distributions during the September 30, 2012, dropout event. The format is the same as shown in Figure 12.5, except the times listed correspond to when the spacecraft (THEMIS-D or -E) were at geosynchronous orbit. (b) Comparing the percent difference from the THEMIS observations shown in (a) to the results from the simple model shown in Figure 12.3d. For the observations (black line with markers), the pre-dropout distribution was taken from the September 30, 05:30 UT curve and the final from the October 1, 06:30 UT curve. The observed dropout started shortly after 11:00 UT, and the simulation was run for 19 hours with the results from the start and stop times shown here with the solid blue line. Note the dashed line at zero denotes the boundary between increased PSD (positive percentage difference) and decreased PSD (negative percentage difference).*

range of equatorial pitch angles. From PSD analysis, the dropout included actual loss of more than 90% of electrons throughout most of the belt ($L^* > \sim 4$), and the loss was effective over a period of only a few hours ($< \sim 1/2$ day). Losses started first at higher L^* and moved in to lower L^* over time, and the losses were ultimately greatest at higher L-shells. Furthermore, Van Allen Probes revealed that there were similar losses observed in energetic (hundreds of keV to >1 MeV) ring current protons, which also exhibited some of the same characteristics as the electrons (i.e., sharp cutoffs in the radial distributions following sudden inward magnetopause motion, loss starting at high L-shells and moving in over time, and stronger losses at higher L-shells). Turner et al. [2014] concluded that the only loss mechanism theory that can explain simultaneously all of these features is magnetopause shadowing and subsequent outward radial transport. However, Van Allen Probes revealed notably different results for $L^* < 4$. There, additional losses of predominantly very high-energy (i.e., multi-MeV), high-K (i.e., mirroring at high magnetic latitudes) electrons were also observed. The energy and pitch angle dependence of the loss explains why it was not observed in the THEMIS results shown in Figure 12.9a (also consistent with Van Allen Probes results, not shown here). Turner et al. [2014] speculated that these losses may have resulted due to atmospheric losses from wave-particle interactions with EMIC waves outside of the plasmapause. If so, this event also provided: (1) evidence of how EMIC waves can result in rapid, energy- and

pitch angle-dependent loss of relativistic electrons; and (2) supporting evidence for the scenario presented in Bortnik et al. [2006], who concluded that loss during dropouts may be L-shell dependent. Loss at higher L-shells (e.g., $L^* > \sim 4$ or 5) can be dominated by outward transport, while at lower L-shells, loss can be dominated by scattering into the atmospheric loss cone.

12.3.2.2 Prolonged depletions

During the previous solar minimum, the relativistic electrons in Earth's outer radiation belt essentially vanished or were at very low intensity throughout all of 2009 and into early 2010. During this period, the solar wind speed and IMF strength were unusually low, with the 27-day averaged speed barely going above 400 km/s and the IMF staying around only 4 nT [Kataoka and Miyoshi, 2010]. Kataoka and Miyoshi [2010] studied this period of prolonged outer belt depletion using GOES data from GEO. They compared the 2009 solar minimum period to that from 1996 to 1997, which also had below-average solar wind levels but did not display the extremely weak outer radiation belt. They concluded that the extremely weak IMF in the recent solar minimum, when combined with the slow solar wind, resulted in lower storm and substorm activity, and was the primary factor in suppressing outer belt source processes and the exceedingly low levels of relativistic electrons there.

Using THEMIS data, Lee et al. [2013] also studied the prolonged outer belt depletion during the last solar minimum. They reported how the outer belt essentially disappeared during several intervals throughout the period, one of which lasted up to two months before a weak form of the belt reformed. They highlighted the importance of outer belt losses during the prolonged depletion period, showing that during the periods where the belt disappeared, the plasmasphere had expanded to high L-shells (beyond GEO). This expansion of the plasmasphere impacted the outer belt in two ways: (1) the supply of tens to hundreds of keV electrons from the plasma sheet due to energetic particle injections and enhanced convection (e.g., Figure 12.2) was greatly diminished, affecting outer belt source processes; and (2) loss processes due to pitch angle scattering from interactions with hiss waves within the highly inflated plasmasphere [e.g., Lyons and Thorne, 1973] were effective throughout the vast majority of the outer belt. Thus, the prolonged depletion of the outer belt around 2009 provided an excellent opportunity to understand the extreme effects that can result from longer-term competition between source and loss processes of the outer belt electrons.

12.3.3 Complex outer belt structures: remnant belts

We next review one more type of extreme variation of the outer belt electrons, since it likely results due to a dynamic interplay of several of the loss and source processes discussed in this paper. Baker et al. [2013] and Turner et al. [2013] independently reported two different cases of a bifurcation of the outer radiation belt, in which the belt exhibited two distinct peaks in intensity of relativistic electrons. Typically, the outer radiation belt has a single peak in intensity, somewhere between $4 < L < 6$. However, shortly after the launch of the Van Allen Probes, the spacecraft observed a dropout on September 3, 2012, which left in its wake a remnant belt of several MeV electrons between

$\sim 3 < L < \sim 3.5$. However, over the next several days, another belt started forming at higher L ($L > \sim 4$) resulting in two distinct peaks in intensity separated by a second slot region [Baker et al., 2013]. The double outer belt structure persisted for over 25 days at multi-MeV energies, until another dropout occurred on September 30, 2012 (see details of that dropout above). Examining the formation and decay of the innermost of the two belts, Thorne et al. [2013a] showed that the belt formed over a broader range of energy than was observable with the Van Allen Probes REPT instruments [Baker et al., 2012], down to at least 300 keV as observed by THEMIS. However, the innermost belt exhibited an energy-dependent decay, which Thorne et al. [2013] showed was due to energy-dependent losses due to interactions with plasmaspheric hiss. This explained the THEMIS observations and why the lower-energy MagEIS instruments [Blake et al., 2013] did not observe the double outer belt structure when those instruments were turned on later in September. Baker et al. [2013] and Thorne et al. [2013a] demonstrated the importance of the plasmasphere in the formation of such a complex outer belt structure.

Using THEMIS observations, Turner et al. [2013] studied a separate instance of a double outer belt structure that occurred on February 2, 2011. Like the September 2013 event, this double outer belt structure formed after an outer belt dropout. However, Turner et al. [2013] examined relativistic electron PSD for fixed values of the first and second adiabatic invariants, which provided further insight into the nature of the formation of the double outer belt. Figure 12.10 showcases their results. Before the

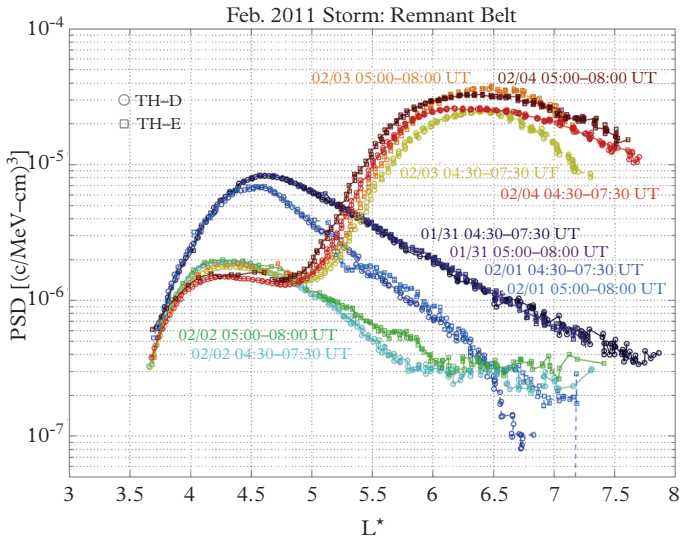

Figure 12.10 *Phase space density distributions from the February 2011 remnant belt event. The format is the same as that used for Figure 12.5 with the corresponding times shown on the plot. This period reveals how a double outer belt structure could form out of the remnant belt after a dropout.*

event, the outer belt PSD distribution in L^* for electrons with μ = 1000 MeV/G and K < 0.025 $G^{1/2}R_E$ was peaked around $L^* \sim 4.5$, as shown with the dark blue curve from early in the day on January 31, 2011. Following a sudden increase in the solar wind dynamic pressure and magnetopause compression on January 31, there was an outer radiation belt dropout. During the dropout, the peak in PSD decreased and moved closer to $L^* \sim 4$ and the losses started at higher L^* and moved to lower L^* over time, as seen from the blue and cyan curves in Figure 12.10. As we discussed earlier in this paper, these signatures are typical of dropouts dominated by losses from magnetopause shadowing and outward radial transport. The remnant belt after this dropout is shown in the green curve from February 2, 2011, on Figure 12.10. However, within less than 24 hours, a new outer belt formed at higher L^*, evidently independent of the remnant belt. This resulted in a double peaked PSD distribution shown in the yellow, orange, and red curves. The two peaks were even more pronounced in flux observations. Based on estimates of the plasmapause from this period, this new outer belt formed just outside of the plasmapause, which had expanded out to $L^* > 4.5$ on February 2. The slow decay in the remnant belt from February 2 to 4 is also consistent with slow losses due to plasmaspheric hiss, as was shown for the September 2012 case by Thorne et al. [2013]. Turner et al. [2013] also showed that this new outer belt formed over the same period and at the same L^* range in which the peak chorus wave activity was observed. This double outer belt structure was eradicated by another dropout event during the February 4, 2011, storm event discussed in Section 12.3.1.1.

These two events showcase how the various source, loss, and transport processes discussed here, combined with the nature of the plasmasphere, can conspire to result in the formation of two outer radiation belts. The dropout at the beginning of the formation is necessary to produce the remnant belt of electrons, which will later become the inner of the two outer radiation belts. If the plasmapause then expands rapidly outward over the next day or so, this remnant belt is essentially shielded by the plasmasphere, within which ULF activity is damped so inward radial diffusion from the new outer belt that forms outside the plasmapause cannot rapidly engulf the remnant belt's peak. Within the plasmasphere, those electrons in the remnant belt are primarily affected by slow, energy-dependent decay due to interactions with plasmaspheric hiss. The plasmapause also serves as a critical boundary for the formation of the new belt at higher L^*. Chorus waves outside of the plasmapause can accelerate a seed population of freshly injected tens to hundreds of keV electrons up to relativistic energies, resulting in the formation of the new belt. This formation scenario was confirmed by the three-dimensional modeling effort presented in Shprits et al. [2013], who successfully simulated the evolution of the September 2012 "storage ring" event.

12.4 Outstanding questions and topics for future work

In the last two decades, the radiation belt community has conducted an overhaul in the theoretical framework of the drivers of extreme variations of relativistic electrons in Earth's outer radiation belt. However, many important questions of increasing specificity

regarding the processes at work remain. Thanks to the unprecedented level and quality of observations by missions like NASA's Van Allen Probes and THEMIS the field has the potential of addressing these questions and usher a qualitative change in our understanding of outer radiation belt dynamics. Next, we highlight just a few of the many outstanding questions and topics that may prove important to further understanding extreme variations of Earth's outer belt electrons.

12.4.1 Concerning sources

We have stressed here the importance of energetic particle injections and local acceleration to enhancements of the outer radiation belt. One major outstanding question concerning the role of energetic electron injections is: What is the upper energy threshold of energetic electron injections, and how does this change with various activity indicators? As Ingraham et al. [2001] showed, direct injections of ~MeV electrons may be possible following periods of sustained substorm activity. Also, Figure 12.8 shows GOES observations of how the upper energy threshold of injected electrons increases during subsequent injections. It is important to understand the processes active in the magnetotail responsible for this acceleration of plasma sheet electrons and the extent to which this acceleration can be effective. Since it is injected electrons that form the source and seed populations for local acceleration by wave-particle interactions within the heart of the outer belt (e.g., Figure 12.2), a higher upper energy threshold on the injected electrons may play a critical role in enabling that local acceleration to be more effective for reaching higher energy levels over shorter timescales.

Another question that may prove to be important to sudden enhancements, or depletions, of radiation belt electrons is: How important is the role of nonlinear wave-particle interactions between whistler-mode waves and energetic electrons for acceleration and/or loss? Large amplitude whistler waves have been observed in Earth's outer radiation belts [e.g., Wilson et al., 2011]. Such waves invalidate several of the assumptions fundamental to quasilinear diffusion theory, and with test-particle simulations, researchers have only started to study how interactions with such nonlinear waves can affect outer belt electrons. Albert [2002] found that phase-bunching during wave-particle interactions can lead to deceleration, while phase-trapping leads to very rapid acceleration of a small number of the test particles. Bortnik et al. [2008] found similar results, though added that the type of interaction may be dependent on the latitude (and thus wave normal angle) at which it takes place. Tao et al. [2012] examined the effects of amplitude modulation in electron interactions with chorus waves. They found that amplitude modulation—as is observed in chorus wave packets—has a significant effect on phase-bunching and phase-trapping during the interactions. These results demonstrate the complexity of wave-particle interactions and the necessity for better understanding their role in accelerating and scattering outer belt electrons.

12.4.2 Concerning losses

Many questions still remain on the nature of losses of electrons through the magnetopause. For example, is electron loss through the magnetopause like an open drain that

always operates or is it dependent on magnetic connection to the magnetosheath? This is a complex question, and it has significant implications for loss of electrons from the outer radiation belt since the relativistic population typically has a negative PSD gradient beyond GEO and radial diffusion is faster at higher L-shells (as discussed throughout this chapter). If the magnetopause was just a constant sink for electrons, then it should play a major role in controlling the population at lower L-shells: in particular it could limit the PSD gradient and the maximum height of the PSD peak at lower L-shells. This limit would also depend on the radial diffusion coefficient due to magnetospheric wave activity. However, the magnetopause is an ion scale layer, and when low-latitude reconnection is not occurring on the dayside (i.e., periods of northward IMF), the equatorial magnetopause is a tangential discontinuity with no magnetic connection to the magnetosheath. So, is it possible for outer belt electrons to escape through the magnetopause under northward IMF conditions? The answer to this might be dependent on the electron energy; if the electron gyro-radius is large enough (i.e., the electron is energetic enough) to be comparable to the thickness of the magnetopause, then they might escape. This should prove to be an interesting topic for future work.

Shprits et al. [2012] studied dropouts during the CRRES period and showed that 22 of 25 dropouts (88%) were associated with enhancements in solar wind dynamic pressure just prior to the event. The remaining three cases occurred under relatively steady solar wind dynamic pressure. This raises the question: What causes outer belt dropouts that are not related to magnetopause shadowing events? EMIC waves may play a dominant role in those other events, and they may also contribute to the magnetopause shadowing events as well, as was indicated by Bortnik et al. [2006] and Turner et al. [2014]. Therefore, it would be important to study how many dropout events include losses due to EMIC waves and over what ranges of L-shells, pitch angles, and energies are those losses effective. The latter is a question that will require multipoint observations, combining simultaneous measurements from equatorial, high-altitude and polar, LEO satellites to address.

12.4.3 Concerning transport

Claudepierre et al. [2013] showed evidence of resonant interactions between ~60 keV drifting electrons and poloidal ULF waves. Theoretically, drift resonance between electrons and ULF waves could lead to rapid acceleration of outer belt electrons [e.g., Elkington et al., 2003]. However, observational evidence of such a mechanism has proven elusive, so the question remains as to the importance of drift resonance in relativistic electron acceleration in the outer belt. New observations from the Van Allen Probes, which provide an unprecedented level of energy resolution, should help address this question.

Significant effects from transport can also occur around locations where the global magnetic field varies from its typical, dipole-like geometry, and there are many outstanding questions concerning such scenarios. For example, the test-particle simulations by Ukhorskiy et al. [2011] demonstrated that electrons may experience significant transport in L and sudden scattering in pitch angle when they undergo bifurcated drift orbits, yet

there has not been a thorough observational analysis of the effects of such orbits on outer belt electrons drifting at high L-shells. THEMIS provides a near-ideal dataset for such an analysis, since it provides multipoint, pitch-angle resolved observations of energetic electrons near the magnetic equator from high L-shells on the dayside. The ring current and partial ring current also play a role in altering the drift trajectories of outer belt electrons [e.g., Ukhorskiy et al., 2006], which is another topic with several interesting areas for future research using multipoint observations.

12.5 Conclusions

This chapter focused on extreme variations of the outer radiation belt electrons from a primarily observational standpoint. We have provided a brief history of the topic as well as an overview of the current understanding concerning processes that result in the drastic enhancements and depletions that are observed so often in relativistic electron intensity in the outer belt. Furthermore, we have presented some recent example cases of sudden enhancements, injections from interplanetary shock impacts, energetic electron injections associated with dipolarization fronts, flux dropout events, prolonged depletions, and double outer belt structures that can form out of the remnant belt population after dropouts. These examples showcase how, with the availability of an unprecedented number of spacecraft observing the outer belt electrons simultaneously, we are currently in a "golden era" for radiation belt physics. Multipoint observations from missions like NASA's THEMIS and Van Allen Probes have already provided strong evidence addressing previous outstanding questions such as the dominant acceleration mechanism for relativistic electrons or the dominant loss mechanism during dropouts. However, many outstanding questions remain as indicated in the previous section.

Despite our current level of understanding, the ability to predict how the outer belt will respond to given solar wind inputs for individual events has proven exceedingly challenging. Currently, radiation belt models are able to reasonably predict the longer-term climatology or reproduce individual events after their outcomes were already observed. The challenge of predicting the extreme variability of the outer belt is an outcome of the belt's very nature: outer belt variations are the result of a complex interplay between multiple source, loss, and transport processes. The picture is further complicated by the often-random individual outcomes of each of those processes provided similar input conditions. In many ways the system is analogous to terrestrial weather: a complex set of often coupled driving processes results in chaotic responses of the system. However, terrestrial weather has proven that some level of predictability is possible. That predictability is provided by coupling complex global models which capture or otherwise parameterize all of the underlying physics, with a global network of observatories which provide the models with input data in near real time. Therefore, we must continue pushing our model capabilities while simultaneously increasing the number of observation points throughout the system.

Acknowledgments

D. L. Turner and V. Angelopoulos are thankful for funding support from NASA (THEMIS mission: contract NAS5-02099; and a grant: NNX12AJ55G) and the Monitoring, Analyzing, and Assessing the Radiation Belt Loss and Energization (MAARBLE) project funded under the European Commission's (EC) FP7 framework (note that this work reflects the authors' views, and the EC is not liable for any use that may be made of the information contained herein). We would also like to thank the THEMIS and Van Allen Probes teams, NOAA's NGDC and NASA's CDAWeb online databases, the SpacePy (http://spacepy.lanl.gov/) development team, and the THEMIS Data Analysis Software (TDAS: http://themis.ssl.berkeley.edu/software.shtml) development team.

REFERENCES

Albert, J. M. (2002), Nonlinear interaction of outer zone electrons with VLF waves, *Geophys. Res. Lett.*, **29**, 8, doi:10.1029/2001GL013941.

Albert, J. M. (2003), Evaluation of quasi-linear diffusion coefficients for EMIC waves in a multispecies plasma, *J. Geophys. Res.*, **108** (A6), 1249, doi:10.1029/2002JA009792.

Allen, R. C., et al. (2013), Multiple bidirectional EMIC waves observed by Cluster at middle magnetic latitudes in the dayside magnetosphere, *J. Geophys. Res. Space Physics*, 118, doi:10.1002/jgra.50600.

Angelopoulos, V. (2008), The THEMIS Mission, *Space Sci. Rev.*, **141**, 5–34, doi:10.1007/s11214-008-9336-1.

Angelopoulos, V. (2011), The ARTEMIS Mission, *Space Sci. Rev.*, **165**, 3–25, doi:10.1007/s11214-010-9687-2.

Angelopoulos, V., et al. (2013), Electromagnetic energy conversion at reconnection fronts, *Science*, **341**, 1478, doi:10.1126/science.1236992.

Artemyev, A. V., O. V. Agapitov, D. Mourenas, V. Krasnoselskikh, and L. M. Zelenyi (2013), Storm-induced energization of radiation belt electrons: Effect of wave obliquity, *Geophys. Res. Lett.*, **40**, doi:10.1002/grl.50837.

Baker, D. N., J. B. Blake, L. B. Callis, R. D. Belian, and T. E. Cayton (1989), Relativistic electrons near geostationary orbit: Evidence for internal magnetospheric acceleration, *Geophys. Res. Lett.*, **16**, 559.

Baker, D. N., et al. (1994), Relativistic electron acceleration and decay time scales in the inner and outer radiation belts: SAMPEX, *Geophys. Res. Lett.*, **21**, 6, 409–412.

Baker, D. N., S. G. Kanekal, X. Li, S. P. Monk, J. Goldstein, and J. L. Burch (2004), An extreme distortion of the Van Allen belt arising from the 'Hallowe'en' solar storm in 2003, *Nature*, **432**, 878–881.

Baker, D. N., et al. (2012), The Relativistic Electron-Proton Telescope (REPT) instrument on board the Radiation Belt Storm Probes (RBSP) spacecraft: Characterization of Earth's radiation belt high-energy particle populations, *Space Sci. Rev.*, **179**, 337–381, doi:10.1007/s11214-012-9950-9.

Baker, D. N., et al. (2013), A long-lived relativistic electron storage ring embedded in Earth's outer Van Allen Belt, *Science*, **340**, doi:10.1126/science.1233518.

Baker, D. N., et al. (2014), Gradual diffusion and punctuated phase space density enhancements of highly relativistic electrons: Van Allen Probes observations, *Geophys. Rev. Lett.*, **41**, doi:10.1002/2013GL058942.

Birn, J., M. F. Thomsen, J. E. Borovsky, G. D. Reeves, D. J. M. R. D. Belian, and M. Hesse (1997), Substorm ion injections: Geosynchronous observations and test particle orbits in three-dimensional dynamic MHD fields, *J. Geophys. Res.*, **102**, 2325.

Birn, J., et al. (1998), Substorm electron injections: Geosynchronous observations and test particle simulations, *J. Geophys. Res.*, **103**, 9235.

Blake, J. B., W. A. Kolasinski, R. W. Fillius, and E. G. Mullen (1992), Injection of electrons and protons with energies of tens of MeV into L < 3 on March 24, 1991, *Geophys. Res. Lett.*, **19**, 8, 821–824.

Blake, J. B., et al. (1995), CEPPAD: Comprehensive energetic particle and pitch angle distribution experiment on POLAR, *Space Sc. Rev.*, **71**, 531–562.

Blake, J. B., et al. (2013), The Magnetic Electron Ion Spectrometer (MagEIS) instruments aboard the Radiation Belt Storm Probes (RBSP) spacecraft, *Space Sci. Rev.*, **179** (1–4), 383–421, doi:10.1007/s11214-013-9991-8.

Borovsky, J. E. and M. Denton (2009), Relativistic-electron dropouts and recovery: A superposed epoch study of the magnetosphere and solar wind, *J. Geophys. Res.*, **114**, A02201, doi:10.1029/2008JA013128.

Bortnik, J., et al. (2006), Observation of two distinct, rapid loss mechanisms during the November 20, 2003, radiation belt dropout event, *J. Geophys. Res.*, **111**, A12216, doi:10.1029/2006JA011802.

Bortnik, J., R. M. Thorne, and U. S. Inan (2008), Nonlinear interaction of energetic electrons with large amplitude chorus, *Geophys. Res. Lett.*, **35**, L21102, doi:10.1029/2008GL035500.

Boyd, A. J., et al. (2014), Quantifying the radiation belt seed population in the March 17, 2013, electron acceleration event, *Geophys. Res. Lett.*, **41**, doi:10.1002/2014GL059626.

Brautigam, D. H. and J. M. Albert (2000), Radial diffusion analysis of outer radiation belt electrons during the October 9, 1990, magnetic storm, *J. Geophys. Res.*, **105** (A1), 291–309.

Claudepierre, S. G., et al. (2013), Van Allen Probes observation of localized drift resonance between poloidal mode ultra-low frequency waves and 60 keV electrons, *Geophys. Res. Lett.*, **40**, doi:10.1002/grl.50901.

Chen, Y., G. D. Reeves, and R. H. W. Friedel (2007), The energization of relativistic electrons in the outer Van Allen radiation belt, *Nat. Phys.*, doi:10.1038/nphys655.

Craven, J. D. (1966), Temporal variations of electron intensities at low altitudes in the outer radiation zone as observed with satellite Injun 3, *J. Geophys. Res.*, **71**, 5643–5663.

Desorgher, L., P. Bühler, A. Zehnder, and E. O. Flückiger (2000), Simulation of the outer radiation belt electron flux decrease during the March 26, 1995, magnetic storm, *J. Geophys. Res.*, **105** (A9), 21,211–21,223, doi:10.1029/2000JA900060.

Dessler, A. J. and R. Karplus (1961), Some effects of diamagnetic ring currents on Van Allen radiation, *J. Geophys. Res.*, **66**, 8, 2289–2295.

Elkington, S. R., M. K. Hudson, and A. A. Chan (2003), Resonant acceleration and diffusion of outer zone electrons in an asymmetric geomagnetic field, *J. Geophys. Res.*, **108** (A3), 1116, doi:10.1029/2001JA009202.

Friedel, R. H. W., G. D. Reeves, and T. Obara (2002), Relativistic electron dynamics in the inner magnetosphere – a review, *J. Atmos. Sol.-Terr. Phys.*, **64**, 265–682.

Fujimoto, M. and A. Nishida (1990), Energization and anisotropization of energetic electrons in the Earth's radiation belt by the recirculation process, *J. Geophys Res.*, **95**, 4265.

Gabrielse, C., V. Angelopoulos, A. Runov, and D. L. Turner (2012), The effects of transient, localized electric fields on equatorial electron acceleration and transport toward the inner magnetosphere, *J. Geophys. Res.*, **117**, A10213, doi:10.1029/2012JA017873.

Green, J. C. and M. G. Kivelson (2004), Relativistic electrons in the outer radiation belt: Differentiating between acceleration mechanisms, *J. Geophys. Res.*, **109** (A3), A03213, doi:10.1029/2003JA010153.

Green, J. C., T. G. Onsager, T. P. O'Brien, and D. N. Baker (2004), Testing loss mechanisms capable of rapidly depleting relativistic electron flux in the Earth's outer radiation belt, *J. Geophys. Res.*, **109**, A12211, doi:10.1029/2004JA010579.

Horne, R. B. and R. M. Thorne (1998), Potential waves for relativistic electron scattering and stochastic acceleration during magnetic storms, *Geophys. Res. Lett.*, **25** (15), 3011–3014.

Horne, R. B., et al. (2005), Timescale for radiation belt electron acceleration by whistler mode chorus waves, *J. Geophys. Res.*, **110**, A03225, doi:10.1029/2004JA010811.

Horne, R. B. (2007), Acceleration of Killer Electrons, *Nat. Phys.,* **3**, 590–591.

Horne, R. B., M. M. Lam, and J. C. Green (2009), Energetic electron precipitation from the outer radiation belt during geomagnetic storms, *Geophys. Res. Lett.*, **36**, L19104, doi:10.1029/2009GL040236.

Hudson, M. K., B. T. Kress, H.-R. Mueller, J. A. Zastrow, and J. B. Blake (2008), Relationship of the Van Allen radiation belts to solar wind drivers, *J. Atmos. Sol.-Terr. Phys.*, **70**, 708–729, doi:10.1016/j.jastp.2007.11.003.

Hudson, M. K., et al. (2014), Simulated magnetopause losses and Van Allen Probe flux dropouts, *Geophys. Res. Lett.*, **41**, doi:10.1002/2014GL059222.

Ingraham, J. C., et al. (2001), Substorm injection of relativistic electrons to geosynchronous orbit during the great magnetic storm of March 24, 1991, *J. Geophys. Res.*, **106** (A11), 25,759–25,776.

Kataoka, R. and Y. Miyoshi (2008), Average profiles of the solar wind and outer radiation belt during the extreme flux enhancement of relativistic electrons at geosynchronous orbit, *Ann. Geophys.*, **26**, 1335–1339.

Kataoka, R. and Y. Miyoshi (2010), Why are relativistic electrons persistently quiet at geosynchronous orbit in 2009? *Space Weather*, **8**, S08002, doi:10.1029/2010SW000571.

Kim, H.-J. and A. A. Chan (1997), Fully adiabatic changes in storm time relativistic electron fluxes, *J. Geophys. Res.*, **102** (A10), 22107–22116.

Kim, H.-J., E. Zesta, K.-C. Kim, Y. Shprits, Y. Shi, and L. R. Lyons (2010), Estimation of radial gradients of phase space density from POLAR observations during a quiet period prior to a sudden solar wind dynamic pressure enhancement, *J. Geophys. Res.*, **115**, A12249, doi:10.1029/2010JA015722.

Kim, K. C., et al. (2008), Numerical calculations of relativistic electron drift loss effect, *J. Geophys. Res.*, **113**, A09212, doi:10.1029/2007JA013011.

Kim, K. C., D.-Y. Lee, H.-J. Kim, E. S. Lee, and C. R. Choi (2010), Numerical estimates of drift loss and Dst effect for outer radiation belt relativistic electrons with arbitrary pitch angle, *J. Geophys. Res.*, **115**, A03208, doi:10.1029/2009JA014523.

Lee, D.-Y., et al. (2013), Long-term loss and re-formation of the outer radiation belt, *J. Geophys. Res. Space Physics*, **118**, doi:10.1002/jgra.50357.

Li, X., I. Roth, M. Temerin, J. R. Wygant, M. K. Hudson, and J. B. Blake (1993), Simulation of the prompt energization and transport of radiation belt particles during the March 24, 1991, SSC, *Geophys. Res. Lett.*, **20**, 2423–2426, doi:10.1029/93GL02701.

Li, X. et al. (1997), Multisatellite observations of the outer zone electron variation during the November 3–4, 1993, magnetic storm, *J. Geophys. Res.*, **102** (A7), 14123–14140.

Li, X., et al. (1998), Energetic electron injections into the inner magnetosphere during the Jan. 10-11, 1997 magnetic storm, *Geophys. Res. Lett.*, **25**, 2561–2564.

Li, X. and M. A. Temerin (2001), The Electron Radiation Belt, Space Science Reviews, **95** (1/2), 569.

Li, X., et al. (2003a), Energetic particle injections in the inner magnetosphere as a response to an interplanetary shock, *J. Atmos. Sol.-Terr. Phys.*, **65**, 233–244.

Li, X., T. E. Sarris, D. N. Baker, W. K. Peterson, and H. J. Singer (2003b), Simulation of energetic particle injections associated with a substorm on August 27, 2001, *Geophys. Res. Lett.* , **30** (1), 1004, doi:10.1029/2002GL015967.

Li, X., et al. (2009), Modeling the deep penetration of outer belt electrons during the "Halloween" magnetic storm in 2003, *Space Weather*, **7**, S02004, doi:10.1029/2008SW000418.

Li, X., et al. (2013), First results from CSSWE CubeSat: Characteristics of relativistic electrons in the near-earth environment during the October 2012 magnetic storms, *J. Geophys. Res. Space Physics*, **118**, doi:10.1002/2013JA019342.

Li, W. et al. (2009), Global distribution of whistler-mode chorus waves observed on the THEMIS spacecraft, *Geophys. Res. Lett.*, **36**, L09104, doi:10.1029/2009GL037595.

Liu, J., V. Angelopoulos, A. Runov, and X.-Z. Zhou (2013), On the current sheets surrounding dipolarizing flux bundles in the magnetotail: The case for wedgelets, *J. Geophys. Res. Space Physics*, **118**, doi: 10.1002/jgra.50092.

Loto'aniu, T. M., et al. (2010), Relativistic electron loss due to ultralow frequency waves and enhanced outward radial diffusion, *J. Geophys. Res.*, **115**, A12245, doi:10.1029/2010JA015755.

Lyons, L. R. and R. M. Thorne (1973), Equilibrium structure of radiation belt electrons, *J. Geophys. Res.*, 78 (13), 2142–2149.

Matsumura, C., Y. Miyoshi, K. Seki, S. Saito, V. Angelopoulos, and J. Koller (2011), Outer radiation belt boundary location relative to the magnetopause: Implications for magnetopause shadowing, *J. Geophys. Res.*, **116**, A06212, doi:10.1029/2011JA016575.

Mauk, B. H., N. J. Fox, S. G. Kanekal, R. L. Kessel, D. G. Sibeck, and A. Ukhorskiy (2012), Science objectives and rationale for the Radiation Belt Storm Probes mission, *Space Sci. Rev.,* doi:10.1007/s11214-012-9908-y.

McCollough, J. P., S. R. Elkington, and D. N. Baker (2012), The role of Shabansky orbits in compression-related electromagnetic ion cyclotron wave growth, *J. Geophys. Res.*, **117**, A01208, doi:10.1029/2011JA016948.

McIlwain, C. E. (1961), Coordinates for mapping the distribution of magnetically trapped particles, *J. Geophys. Res.*, **66**, 3681.

McIlwain, C. E. (1966a), Ring current effects on trapped particles, *J. Geophys. Res.*, **71** (15), 3623–3628.

McIlwain, C. E. (1966b), Processes acting upon outer zone electrons, *Preprint UCSD-SP-66-5*, Presented at Solar Terrestrial Physics Symposium, Belgrade, 1966.

Meredith, N. P., M. Cain, R. B. Horne, R. M. Thorne, D. Summers, and R. R. Anderson (2003), Evidence for chorus-driven electron acceleration to relativistic energies from a survey of geomagnetically disturbed periods, *J. Geophys. Res.*, **108** (A6), 1248, doi:10.1029/2002JA009764.

Meredith, N. P., R. B. Horne, M. M. Lam, M. Denton, J. E. Borovsky, and J. C. Green (2011), Energetic electron precipitation during high-speed solar wind stream driven storms, *J. Geophys. Res.*, **116**, A05223, doi:10.1029/2010JA016293.

Millan, R. M., K. B. Yando, J. C. Green, and A. Y. Ukhorskiy (2010), Spatial distribution of relativistic electron precipitation during a radiation belt depletion event, *Geophys. Res. Lett.*, **37**, L20103, doi:10.1029/2010GL044919.

Millan, R. M. and R. M. Thorne (2007), Review of radiation belt relativistic electron losses, *J. Atmos. Sol.-Terr. Phys.*, **69**, doi:10.1016/j.jastp.2006.06.019.

Millan, R. M. and D. N. Baker (2012), Acceleration of particles to high energies in Earth's radiation belts, *Space Sci. Rev.*, **173**, 103–131, doi:10.1007/s11214-012-9941-x.

Morley, S. K., et al. (2010), Dropouts of the outer electron radiation belt in response to solar wind stream interfaces: Global Positioning System observations, *Proc. Roy. Soc. A,* Vol. **466**, 3329–3350, doi:10.1098/rspa.2010.0078.

Northrop, T. G. and E. Teller (1960), Stability of the adiabatic motion of charged particles in the Earth's field, *Phys. Rev.*, **117**, 215–225.

O'Brien, T. P., M. D. Looper, and J. B. Blake (2004), Quantification of relativistic electron microburst losses during the GEM storms, *Geophys. Res. Lett.*, **31**, L04802, doi:10.1029/2003GL018621.

Reeves, G. D., et al. (1998), The relativistic electron response at geosynchronous orbit during the January 1997 magnetic storm, *J. Geophys. Res.*, **103** (A8), 17559–17570.

Reeves, G. D., et al. (2013), Electron acceleration in the heart of the Van Allen radiation belts, *Science*, **341**, 991, doi:10.1126/science.1237743.

Roederer, J. G. (1970), Dynamics of Geomagnetically Trapped Radiation, Springer-Verlag, New York.

Runov, A., V. Angelopoulos, X.-Z. Zhou, X.-J. Zhang, S. Li, F. Plaschke, and J. Bonnell (2011), A THEMIS multicase study of depolarization fronts in the magnetotail plasma sheet, *J. Geophys. Res.*, **116**, A05216, doi:10.1029/2010JA016316.

Russell, C. T. and R. M. Thorne (1970), On the structure of the inner magnetosphere, *Cosmic Electrodynamics*, **1**, 67.

Schiller, Q., X. Li, L. Blum, W. Tu, D. L. Turner, and J. B. Blake (2014), A non-storm time enhancement of relativistic electrons in the outer radiation belt, *Geophys. Rev. Lett.*, **41**, 1–6, doi:10.1002/2013GL058485.

Schulz, M. and L. J. Lanzerotti (1974), Particle Diffusion in the Radiation Belts, Springer-Verlag, New York.

Selesnick, R. S. and J. B. Blake (1997), Dynamics of the outer radiation belt, *Geophys., Res. Lett.*, **24**, 11, 1347–1350.

Selesnick, R. S. and J. B. Blake (2000), On the source location of radiation belt relativistic electrons, *J. Geophys. Res.*, **105** (A2), 2607–2624.

Selesnick, R. S. (2006), Source and loss rates of radiation belt relativistic electrons during magnetic storms, *J. Geophys. Res.*, **111**, A04210, doi:10.1029/2005JA011473.

Shabansky, V. P. (1971), Some processes in magnetosphere, *Space Sci. Rev.*, **12** (3), 299.

Shprits, Y. Y., et al. (2006a), Acceleration mechanism responsible for the formation of the new radiation belt during the 2003 Halloween solar storm, *Geophys. Res. Lett.* **33**, L05104, doi:10.1029/2005GL024256.

Shprits, Y. Y., et al. (2006b), Radial diffusion driven by losses at magnetopause, *J. Geophys. Res.*, **111**, A11214, doi:10.1029/2006JA011657.

Shprits, Y. Y., N. P. Meredith, and R. M. Thorne (2007), Parameterization of radiation belt electron loss timescales due to interactions with chorus waves, *Geophys. Res. Lett.*, **34**, L11110.

Shprits, Y. Y., S. R. Elkington, N. P. Meredith, and D. Subbotin (2008a), Review of modeling losses and sources of relativistic electrons in the outer radiation belt I: Radial transport, *J. Atmos. Sol.-Terr. Phys.*, **70**, doi:10.1016/j.jastp.2008.06.008.

Shprits, Y. Y., D. Subbotin, N. P. Meredith, and S. R. Elkington (2008b), Review of modeling of losses and sources of relativistic electrons in the outer radiation belt II: Local acceleration and loss, *J. Atmos. Sol.-Terr. Phys.*, **70**, doi:10.1016/j.jastp.2008.06.014.

Shprits, Y. Y., M. Daae, and B. Ni (2012), Statistical analysis of phase space density buildups and dropouts, *J. Geophys. Res.*, **117**, A01219, doi:10.1029/2011JA016939.

Shprits, Y. Y., et al. (2013), Unusual stable trapping of ultrarelativistic electrons in the Van Allen radiation belts, *Nat. Phys.*, **9**, doi:10.1038/NPHYS2760.

Su, Z., F. Xiao, H. Zheng, and S. Wang (2011), Radiation belt electron dynamics driven by adiabatic transport, radial diffusion, and wave-particle interactions, *J. Geophys. Res.*, **116**, A04205, doi:10.1029/2010JA016228.

Summers, D., R. M. Thorne, and F. Xiao (1998), Relativistic theory of wave-particle resonant diffusion with application to electron acceleration in the magnetosphere, *J. Geophys. Res.*, **103** (A9), 20487–20500.

Tao, X., J. Bortnik, R. M. Thorne, J. M. Albert, and W. Li (2012), Effects of amplitude modulation on nonlinear interactions between electrons and chorus waves, *Geophys. Res. Lett.*, **39**, L06102, doi:10.1029/2012GL051202.

Temerin, M., I. Roth, M. K. Hudson, J. R. Wygant (1994), New paradigm for the transport and energization of radiation belt particles (abstract), *Eos. Trans. AGU*, **75**, Fall Meet. Suppl., 538, 1994.

Thorne, R. M., R. B. Horne, V. K. Jordanova, J. Bortnik, and S. Glauer (2006), Interaction of EMIC waves with thermal plasma and radiation belt particles, in *Magnetospheric ULF Waves: Synthesis and New Directions* (eds. K Takahashi, P. J. Chi, R. E. Denton, and R. L. Lysak), AGU Monograph Series, Washington D. C., doi:10.1029/169GM14.

Thorne, R. M., et al. (2013a), Evolution and slow decay of an unusual narrow ring of relativistic electrons near L ~ 3.2 following the September 2012 magnetic storm, *Geophys. Res. Lett.*, **40**, doi:10.1002/grl.50627.

Thorne et al. (2013b), Rapid acceleration of relativistic radiation belt electrons by magnetospheric chorus, *Nature*, **504**, doi:10.1038/nature12889.

Tsyganenko, N. A. and M. I. Sitnov (2005), Modeling the dynamics of the inner magnetosphere during strong geomagnetic storms, *J. Geophys. Res.*, **110**, A03208, doi:10.1029/2004JA010798.

Tu, W., R. S. Selesnick, X. Li, and M. D. Looper (2010), Quantification of the precipitation loss of radiation belt electrons observed by SAMPEX, *J. Geophys. Res.*, **115**, A07210, doi:10.1029/2009JA014949.

Turner, D. L. and X. Li (2008), Radial gradients of phase space density of the outer radiation belt electrons prior to sudden solar wind pressure enhancements, *Geophys. Res. Lett.*, **35**, L18101, doi:10.1029/2008GL034866.

Turner, D. L., X. Li, G. D. Reeves, and H. J. Singer (2010), On phase space density radial gradients of Earth's outer-belt electrons prior to sudden solar wind pressure enhancements: Results from distinctive events and a superposed epoch analysis, *J. Geophys. Res.*, **115**, A01205, doi:10.1029/2009JA014423.

Turner, D. L., S. Morley, Y. Miyoshi, B. Ni, and C.-L. Huang (2012a), Outer radiation belt flux dropouts: Current understanding and unresolved questions, in *Dynamics of Earth's Radiation Belts and Inner Magnetosphere* (eds. D. Summers, I. R. Mann, D. N. Baker, and M. Schulz), pp. 195–212, AGU Geophysical Monograph Series, Vol. 199, Washington, D.C., doi:10.1029/2012GM001310.

Turner, D. L., V. Angelopoulos, Y. Shprits, A. Kellerman, P. Cruce, and D. Larson (2012b), Radial distributions of equatorial phase space density for outer radiation belt electrons, *Geophys. Res. Lett.*, **39**, L09101, doi:10.1029/2012GL051722.

Turner, D. L., Y. Y. Shprits, M. Hartinger, and V. Angelopoulos (2012c), Explaining sudden losses of relativistic electrons during geomagnetic storms, *Nat. Phys.*, **8**, doi:10.1038/NPHYS2185.

Turner, D. L., V. Angelopoulos, W. Li, M. D. Hartinger, M. Usanova, I. R. Mann, J. Bortnik, and Y. Shprits (2013), On the storm-time evolution of relativistic electron phase space density in Earth's outer radiation belt, *J. Geophys. Res. Space Physics*, **118**, 2196–2212, doi:10.1002/jgra.50151.

Turner, D. L., et al. (2014), On the cause and extent of outer radiation belt losses during the September 30, 2012, dropout event, *J. Geophys. Res.*, **119**, doi:10.1002/2013JA019446.

Ukhorskiy, A. Y., B. J. Anderson, P. C. Brandt, and N. A. Tsyganenko (2006), Storm time evolution of the outer radiation belt: Transport and losses, *J. Geophys. Res.*, **111**, A11S03, doi:10.1029/2006JA011690.

Ukhorskiy, A. Y., Y. Y. Shprits, B. J. Anderson, K. Takahashi, and R. M. Thorne (2010), Rapid scattering of radiation belt electrons by storm-time EMIC waves, *Geophys. Res. Lett.*, **37**, L09101, doi:10.1029/2010GL042906.

Ukhorskiy, A. Y., M. I. Sitnov, R. M. Millan, and B. T. Kress (2011), The role of drift orbit bifurcations in energization and loss of electrons in the outer radiation belt, *J. Geophys. Res.*, **116**, A09208, doi:10.1029/2011JA016623.

Ukhorskiy, A. Y. and M. I. Sitnov (2012), Dynamics of radiation belt particles, *Space Sci. Rev.*, **179** (1–4), 545–578, doi:10.1007/s11214-012-9938-5.

Van Allen, J. A. and L. A. Frank (1959), Radiation around the Earth to a radial distance of 107,400 km, *Nature*, **183**, 430–434.

Van Allen, J. A. (1969), Charged particles in the magnetosphere, *Rev. Geophys.*, 7 (1, 2), 233–255.

Vernov, S. N. and A. E. Chudukov (1960), Investigation of radiation in outer space, Moscow Cosmic Ray Conference, in Syrovatsky, S.I. (Ed.), *Proceedings of the Moscow Cosmic Ray Conference*, Vol. III, International Union of Pure and Applied Physics, Moscow, p. 19.

Vernov, S. N., V. M. Driatsky, S. N. Kuznetsov, Yu. I. Logachev, E. N. Sosnovets, and V. G. Stolpovsky (1966), Behavior of radiation belts and anomalous absorption of cosmic radiation in the auroral zone during magnetic storms in February 1964, *Geomagn. Aeronomy*, **6**, 1–6.

Vernov, S. N. (1968), The earth's radiation belts, *Ann. IQSY*, **4**.

Vernov, S. N., E. V. Gorchakov, S. N. Kuznetsov, Yu. I. Logachev, E. N. Sosnovets, and V. G. Stolpovsky (1969), Particle fluxes in the outer geomagnetic field, *Rev. Geophys.*, 7 (1, 2), 257–280.

Williams, D. J., J. F. Arens, and L. J. Lanzerotti (1968), Observations of trapped electrons at low and high altitudes, *J. Geophys. Res.*, **73**, 5673–5696.

Wilson, L. B., III, et al. (2011), The properties of large amplitude whistler mode waves in the magnetosphere: Propagation and relationship with geomagnetic activity, *Geophys. Res. Lett.*, **38**, L17107, doi:10.1029/2011GL048671.